*Clays and Clay Minerals* (2026), **74**, e5, 1–16
doi:10.1017/cmn.2026.10022

**Original Paper**

# The effects of bentonite characteristics and buffer solution composition on the adsorption of aflatoxin B1

Aleksandra Daković[1], Marija Marković[1], Milica Ožegović[1], George E. Rottinghaus[2], Milena Obradović[1], Danina Krajišnik[3], Danijela Smiljanić[1], David L. Bish[4] and Jugoslav Krstić[5]

[1]Institute for Technology of Nuclear and Other Mineral Raw Materials, Bulevar Franše d'Eperea 86, 11000 Belgrade, Serbia; [2]Veterinary Medical Diagnostic Laboratory, College of Veterinary Medicine, University of Missouri, Columbia, MO 65211, USA; [3]Department of Pharmaceutical Technology and Cosmetology, University of Belgrade – Faculty of Pharmacy, 11221 Belgrade, Serbia; [4]Department of Chemistry, Indiana University, Bloomington, IN 47405, USA and [5]Institute of Chemistry, Technology and Metallurgy, Institute of National Importance for the Republic of Serbia, University of Belgrade, Njegoševa 12, 11000 Belgrade, Serbia

## Abstract

Aflatoxins (AFs) are contaminants of several agricultural crops, and aflatoxin B1 (AFB1) is the most toxic AF and a known carcinogen to humans and animals. A practical solution for decontamination of animal feed contaminated with AFB1 is to use bentonite, a natural raw material consisting primarily of the mineral montmorillonite (dioctahedral 2:1 layer aluminosilicate of the smectite group). The aims of this research were to compare mineralogical, structural, chemical, and physico-chemical characteristics of three bentonites from the Balkan region (Beretnica clay from Serbia (B-Clay), Yellow clay (Y-Clay) and Gray clay (G-Clay) from Bosnia) with the characteristics of a commercial pharmaceutical-grade bentonite (P-Clay), and to study the behavior of the bentonites in phosphate buffer at pH 3 and 7 with and without AFB1. AFB1 adsorption by bentonites followed non-linear isotherms with maximum amounts adsorbed from 75.43 mg $g^{-1}$ at pH 3 and 62.91 mg $g^{-1}$ at pH 7 for the P-Clay to 100.25 mg $g^{-1}$ at pH 3 and 78.58 mg $g^{-1}$ at pH 7 for the B-Clay. The Ca-bentonites (B-Clay-*cis*-vacant, 83% montmorillonite; Y-Clay-*cis/trans*-vacant, 98% montmorillonite; and G-Clay-*trans*-vacant, 88% montmorillonite) were efficient adsorbents of AFB1, with the greater adsorption observed at pH 3. The P-Clay (Na/Ca bentonite, *cis*-vacant, 63% montmorillonite), exhibited the lowest AFB1 adsorption at both pH values. The behavior of bentonites in buffers, in the presence of AFB1, indicated that ion exchange and AFB1 adsorption by montmorillonite occurred simultaneously. Cations with larger hydrated radii ($Mg^{2+}$ and $Ca^{2+}$) represented the primary active sites for AFB1 adsorption. The position of $OH^-$ groups in *cis*-montmorillonites at the same side of the octahedral site enhanced AFB1 adsorption, making them more available for protonation of edge sites and subsequent interaction with AFB1. Specific characteristics of the montmorillonite in bentonites play an important role in AFB1 adsorption, although the buffer composition also affects the adsorption process significantly.

**Keywords:** adsorption; aflatoxin B1; bentonite; buffer solutions; montmorillonite

(Received: 17 April 2025; revised: 13 January 2026; accepted: 19 January 2026)

## Introduction

Mycotoxins are secondary metabolites of several fungi that are important environmental and carcinogenic agents occurring worldwide (Siri-anusornsak et al., 2023). Fungal infection and mycotoxin production in cereals can have negative effects on the health and growth performance of animals and the quality of animal feed. Consequently, food contamination with mycotoxins represents a human health problem generating a significant economic impact due to the substantial loss in the quality of the products (Liu et al., 2021; Bettiol et al., 2022). Among all mycotoxins, there are >20 different forms of the naturally occurring aflatoxins (AFs) and they are of major concern in the feed and food-processing industries (Li et al., 2020). Aflatoxins, produced mainly by fungi *Aspergillus flavus* and *Aspergillus parasiticus*, are contaminants of several agricultural crops, mainly maize, peanuts, pistachio nuts, and cottonseed. Maize contamination is a major concern as this crop plays an important role in both the food and feed supply worldwide. Until several years ago, AFs were not recognized as contaminants of large concern for primary production in Europe. However, climate change appears to be increasing their prevalence and significant contamination of maize with AFs was reported in Italy and southern Europe in the years 2003 and 2012 (Battilani et al., 2016). Aflatoxin B1 (AFB1) is the most toxic AF and, according to the International Agency for Research on Cancer (IARC), is classified as carcinogenic to humans and is placed in the most toxic group (group 1) (IARC Monographs on the Evaluation of Carcinogenic Risks to Humans, 1993). As a result of this, researchers worldwide have attempted to find ways to remove AFB1 from feed and food.

Of the various techniques proposed for the decontamination of animal feed contaminated with mycotoxins, adsorption has proven to be the best method (Lian et al., 2019; Li et al., 2020). The role of

**Corresponding author:** Aleksandra Daković, Email: a.dakovic@itnms.ac.rs
**Cite this article:** Daković A., Marković M., Ožegović M., Rottinghaus G.E., Obradović M., Krajišnik D., Smiljanić D., Bish D.L., & Krstić J. (2026). The effects of bentonite characteristics and buffer solution composition on the adsorption of aflatoxin B1. *Clays and Clay Minerals* **74**, e5, 1–16. https://doi.org/10.1017/cmn.2026.10022

© The Author(s), 2026. Published by Cambridge University Press on behalf of The Clay Minerals Society.

various adsorbents (clays, zeolites, yeast cell walls, humic substances, activated carbon, etc.) is to bind mycotoxins in the gastrointestinal tract of animals to prevent their undesirable effects. Clay minerals offer special advantages because they are 'green', non-toxic, have large AFB1 adsorption capacities, are abundant in nature, and are cost effective (Li et al., 2020; Lian et al., 2019; Oguz et al., 2022). Investigations of the applications of clay minerals, mainly montmorillonite (the major component of bentonite), to alleviate AFB1 toxicity began in the late 1980s, and the published literature has focused primarily on *in vitro* studies but also on animal trials (Phillips et al., 1988; Desheng et al., 2005; Phillips et al., 2008; Sun et al., 2020). It has been reported that when bentonite is included in AFB1-contaminated feed, improvements in animal performance or survival ranged from 30 to 100% (Desheng et al., 2005; Dixon et al., 2008). Because of the large adsorption capacity of bentonite for AFB1 (resulting from the dominant montmorillonite), it has been authorized since 2013 in Europe as a feed additive under the category of 'technological additives', substances for reduction of contamination of feed by mycotoxins (AFB1) (1m558) (European Commission, 2013).

Bentonite is a natural raw material that consists largely of the clay mineral, montmorillonite (dioctahedral 2:1 layer aluminosilicate of the smectite group), often containing quartz, feldspars, micas, kaolinite, cristobalite, opaline silica, and zeolites. Strictly speaking, 'bentonite' is a rock term and should not be considered equivalent to montmorillonite or smectite. However, many studies simply report on the interactions of AFB1 with 'bentonite' without regard to the fact that bentonites are polymineralic; the term bentonite was adopted in the present manuscript when referring to descriptions of earlier work. Many *in vitro* studies report large differences in the efficiency of AFB1 adsorption by bentonites from different origins. The mineralogical, structural, and chemical characteristics of montmorillonites, summarized in Fig. 1, have the potential to significantly influence AFB1 adsorption.

The mechanism of AFB1 adsorption by hydrated Na-Ca aluminosilicate (HSCAS), commercially known as Novasil, Ca-montmorillonite clay, involves the formation of mononuclear (bidentate) chelate complexes between metal ions in the clay and the β-dicarbonyl system of the AFB1 molecule (Phillips et al., 1995). The adsorption of AFB1 on HSCAS and collapsed HSCAS (heated at 200°C for 30 min and then heated at 800°C for 1 h) was studied by Grant and Phillips (1998). Those authors found a significant decrease in AFB1 adsorption by collapsed HSCAS consistent with the idea that a majority of the active sites for AFB1 adsorption were in the interlamellar region of montmorillonite. Deng et al. (2012) suggested that the AFB1 adsorption efficiency of smectite was dependent on the type of exchangeable cations and that smectite selectivity for AFB1 could be enhanced or weakened by replacing the interlayer cations. They found that when smectite was saturated with divalent cations that have a smaller hydrated radius (e.g. $Ba^{2+}$), the affinity of smectite for AFB1 increased. Also, the authors reported that smectites with smaller cation exchange capacity (CEC) values (<110 meq 100 $g^{-1}$) were more effective at adsorbing AFB1 than smectites with larger CEC values, suggesting that smectites with lower charge density have more non-polar sites at the interlayer surface available for AFB1 adsorption. D'Ascanio et al. (2019) evaluated hydrothermal (15 samples, Ca-smectites) and sedimentary (14 samples, Na-smectites) bentonites as adsorbents for AFB1, and reported that Na-smectites exhibited greater adsorption of AFB1 than Ca-smectites. Tenorio Arvide et al. (2008) reported that montmorillonites with more Fe and Mg in the octahedral sheet had greater adsorption capacities for AFB1. More recently, Vekiru et al. (2015) showed that the differences in the AFB1 adsorption capacity of smectites can be related to the octahedral structural configuration; *cis*-vacant montmorillonites showed a greater AFB1 adsorption than *trans*-vacant montmorillonites. Kannewischer et al. (2006) suggested that possible sites for AFB1 adsorption onto montmorillonites included its interlayers, external layer surfaces, and edge sites. Based on the observations given above, the influence of mineralogical, structural, chemical, and physico-chemical properties of montmorillonites on AFB1 adsorption is evident. Bentonites described in the literature as AFB1 adsorbents are commonly from different deposits all over the world and are usually used in their original forms. They are, therefore, expected to have differences in terms of the aforementioned properties (particularly their bulk mineralogy). In addition, the properties of a given smectite may vary even within the same deposit, thereby influencing AFB1 adsorption. Many of the above-referenced studies used different solutions (e.g. buffer, distilled water), different initial AFB1 concentrations, different amounts of clays, different contact times, and different temperatures, all of which can give rise to differences in the maximum reported amounts of AFB1 adsorbed.

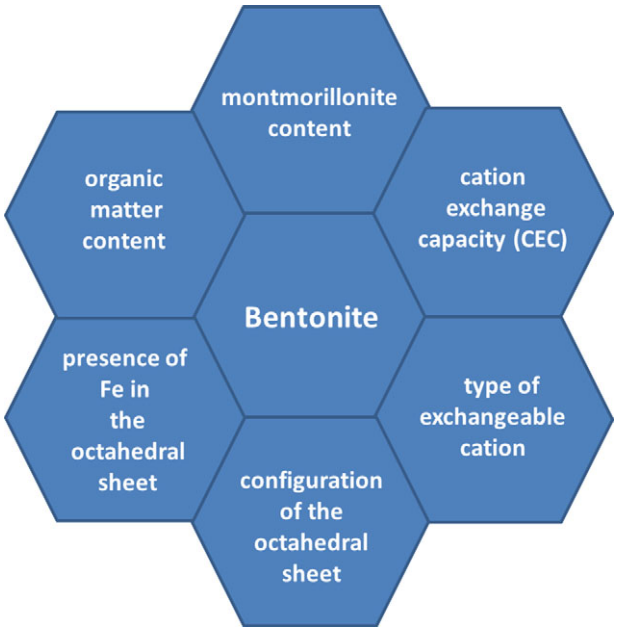



**Figure 1.** Characteristics of bentonites which influence AFB1 adsorption.

Furthermore, only a small number of studies have provided a detailed characterization of the studied bentonites (e.g. their mineralogy) and the behavior of bentonite in the solution in which AFB1 experiments were performed, which together with their efficiencies to bind AFB1 are essential in the prediction of the mycotoxin adsorption mechanism(s). The aim of this research was twofold: (1) to compare mineralogical, structural, chemical, and physico-chemical characteristics of two naturally occurring bentonites from the Balkan region (the Beretnica clay from Serbia (B-Clay) and the Yellow clay from the Šipovo deposit in Bosnia (Y-Clay)) with the characteristics of a pharmaceutical-grade bentonite supplied by Fagron company (P-Clay); and (2) to study the behavior of the bentonites in phosphate buffer at pH 3 and 7 with and without AFB1. Aflatoxin B1 adsorption by bentonites was followed at different levels of each adsorbent in suspension, at different initial AFB1 concentrations, at two pH values, and at

https://doi.org/10.1017/cmn.2026.10022 Published online by Cambridge University Press

fixed contact time (30 min) at room temperature. As bentonites from different parts of the same deposit may have different characteristics and consequently different affinities for AFB1, the previously studied Gray clay from the Šipovo deposit in Bosnia (G-Clay) (Daković et al., 2008; Daković et al., 2012; Shannon et al., 2017) was also included in this research. Characterization of bentonites was done by X-ray diffraction (XRD) analysis, Fourier-transform infrared (FT-IR) spectroscopy, differential thermal analysis (DTA)/thermogravimetry (TG), and by determination of the chemical composition, textural properties as well as CEC and zeta potential. In addition to reporting comparisons between behaviors of the different bentonites towards AFB1, the specific objective of the present research was to provide, for the first time, a more detailed study of the characteristics of bentonites and of their behavior in buffer solutions, emphasizing possible influences on AFB1 adsorption.

## Materials and methods

### Materials and chemicals

Raw bentonites were obtained from the following companies: B-Clay from ZeoWorld LLC and Contractor LLC, Beretnica locality, Republic of Serbia; Y-Clay from Bentoproduct LLC, Šipovo deposit, Bosnia, and G-Clay from Bentonit A.D., Šipovo deposit, Bosnia. To avoid the effects of particle size on AFB1 adsorption, the bentonites were wet sieved to yield uniform <37 μm particles and were then used without further purification. Bentonite of a pharmaceutical grade (P-Clay) was supplied by Fagron company, the Netherlands, and was used without pre-treatment. Aflatoxin B1 was purchased from Romer Labs (Biopure). Acetonitrile, methanol, and water were of HPLC grade and from Honeywell Muskegon, Michigan, USA. Mono- and di-basic potassium phosphate, phosphoric acid, and ammonium chloride were from Sigma-Aldrich Co.

### Characterization of the bentonites

The chemical composition of the wet-sieved bentonites was determined by classical chemical analysis methods for aluminosilicates (Kirschenbaum, 1983). The CEC values of bentonites were determined using the 1 M $NH_4Cl$ method at pH 7. According to this method, 0.5 g of each bentonite was suspended in 50 mL of 1 M $NH_4Cl$ solution and suspensions were shaken for 24 h. Suspensions were then filtered and the exchangeable cations in supernatants were determined. As some bentonites contained carbonate minerals that are soluble in $NH_4Cl$ solution, Ca and Mg were determined in 1 M NaCl following the same procedure. Supernatants from the CEC determination were analyzed by atomic absorption spectroscopy (AAS) (Perkin Elmer, Model 703).

The XRD analysis of the B-Clay, Y-Clay, and P-Clay was performed using a Rigaku SmartLab X-ray diffractometer with CuKα radiation. The XRD data were measured at room temperature from 4 to 65°2θ, with a step size of 0.01°2θ and a time/step of 1 s. *Siroquant* version 4.0 was used for quantitative mineralogical analysis. X-ray diffraction analysis of the G-Clay was done using a Bruker D8 Advance instrument with CuKα radiation and a SolX energy-discriminating point detector.

The FT-IR spectra were obtained using a Thermo Scientific Nicolet iS50 spectrometer in transmission mode. Spectra were recorded over the range 4000–400 $cm^{-1}$ at 64 scans per spectrum at 2 $cm^{-1}$ resolution. A background scan was acquired before scanning the samples. KBr pellets were prepared by mixing 0.2 mg of each clay with 80 mg of dry KBr.

Thermal studies (DTA/TG) were carried out on a STA 449 F5 Jupiter simultaneous thermal analyzer with *Proteus*® software produced by Netzsch, Germany. Samples were heated at a rate of 10°C $min^{-1}$ from 20 to 1000°C using a Pt-Pt10%Rh thermocouple and Pt90Ir10 crucibles with lids. An empty crucible with lid was used as a DTA reference. The oven atmosphere was streamed with 70 mL $min^{-1}$ (20 mL $min^{-1}$ protective gas–synthetic air and 50 mL $min^{-1}$ purge gas–synthetic air). Prior to analysis, samples were kept in a container over a saturated solution of $NH_4Cl$ (relative humidity of 75%) for 24 h.

The zeta potential values were determined using a Zetasizer Nano ZS90 instrument (Malvern Instruments, Malvern, UK). Samples were dispersed in distilled water (0.1 mg $mL^{-1}$) using an ultrasonic bath and operating conditions were adjusted using a calibrated latex dispersion before measurement.

Textural properties of clay samples were determined using $N_2$ adsorption-desorption isotherms obtained at 77K using a Sorptomatic 1990 (Thermo Finnigan) apparatus. Before measurement, the clay sample was degassed at the preparation site for 4 h at room temperature under a vacuum, and then for another 24 h at 373K under a vacuum better than 0.3 Pa. The resultant $N_2$ isotherms were analyzed using the ADP 5.13 Thermo Electron Software. The specific surface areas ($SSA_{N2BET}$) of the samples were calculated using the Brunauer-Emmett-Teller (BET) method (Rouquerol et al., 1999), and the proportion of the adsorption isotherms used for $SSA_{N2BET}$ calculation was selected using the Rouquerol criteria (Rouquerol et al., 2007). The Dubinin-Radushkevich method (Dubinin, 1975) was used to determine the micropore volume ($V_{mic}$); the mesopore volume ($V_{mes}$) was estimated from the adsorption portion of the isotherm for a relative pressure range corresponding to the mesopore region (2–50 nm). The total pore volume ($V_{tot}$) was estimated using the Gurvitch rule (Rouquerol et al., 1999) at $p/p_0$=0.98. The average pore diameter ($D_p$) was calculated using the formula $D_p=4V_{tot}/SSA_{N2BET}$.

### Aflatoxin B1 adsorption experiments

A primary AFB1 stock solution (1000 ppm) was prepared in acetonitrile, and AFB1 test solutions for adsorption studies were prepared by addition of acetonitrile stock solution to 0.1 M phosphate buffer (pH 3, 5, or 7). Adsorption of AFB1, according to the method described by the European Union Regulation (European Commission, 2013), was carried out in phosphate buffer at pH 5 with an AFB1 concentration of 4.0 mg $L^{-1}$ and with 0.02% (w/v) of each adsorbent according to the following procedure: Each adsorbent (100 mg) was suspended in 10 mL of buffer solution and vortexed for 2 min, and 100 μL of each suspension was then added to a 15 mL Falcon tube containing 5 mL of AFB1 test solution (4.0 mg $L^{-1}$). To further investigate the adsorption of AFB1 with different amounts of bentonites, experiments were performed with the same initial concentration of AFB1 and with the following amounts of bentonites: 0.02, 0.01, 0.005, and 0.002% (w/v) in phosphate buffer, at pH 3 and 7. These pH values are typically used to determine the effect of pH on mycotoxin adsorption within the range found in the gastrointestinal tract of monogastric creatures (Merchant et al., 2011; Ožegović et al., 2025). For these investigations, 100, 50, 25, and 10 mg of each bentonite was suspended in 10 mL of buffer solution (pH 3 or 7) and vortexed for

https://doi.org/10.1017/cmn.2026.10022 Published online by Cambridge University Press

2 min, and then 100 µL of suspension of each adsorbent was added to a 15 mL Falcon tube containing 5 mL of AFB1 test solution (4.0 mg $L^{-1}$). Isotherms were measured by dilution of the primary AFB1 stock solution with buffer (pH 3 or 7) to obtain the following AFB1 concentrations: 0.8, 1.6, 2.5, 3.4, 4.3, 5.2, 6.1, 7.0, and 8.0 ppm. Each isothermal point had a total volume of 10 mL of appropriate AFB1 test solution (pH 3 or 7) in a 15 mL Falcon tube in which 200 µL of suspension of each bentonite (0.002% (w/v)) was added.

Buffer solutions were prepared as follows: for pH 3, 13.61 g $KH_2PO_4$ was dissolved in 1.0 L of distilled water to obtain a 0.1 M solution; for pH 5 and 7, the buffer solution consisted of 17.42 g $K_2HPO_4$ dissolved in 1.0 L of distilled water (0.1 M solution). In all cases the pH was adjusted with 1 M $H_3PO_4$.

The behavior of bentonites in buffer solutions without or with AFB1 ($C_0$=8.0 mg $L^{-1}$) was studied by addition of 7 mg of each bentonite to 35 mL of buffer solution – pH 3 or 7 (~0.02% w/v). The concentrations of released cations (Ca, Mg, and Na) as well as concentrations of silica and alumina in the supernatants were determined by AAS.

The suspensions in all experiments were shaken for 30 min at room temperature, and were then centrifuged at 13,000 rpm for 3 min. The initial and final concentrations of AFB1 were determined by high-performance liquid chromatography (HPLC). The Shimadzu HPLC system included a pump LC-20AD, autosampler SIL-20A HT, and fluorescence detector RF-20A ($\lambda_{ex}$=365 nm, $\lambda_{em}$=430 nm). Chromatographic separations were carried out using a Phenomenex column (Hyperclone C18 100×4.6 mm, 3 µm particle size), and the mobile phase was methanol:acetonitrile: water (20:20:60) and was pumped at a flow rate of 1 mL $min^{-1}$. All AFB1 adsorption experiments were carried out in duplicate, and the average values were reported to minimize random measuring error.

## Results and Discussion

### *Characterization of bentonites*

#### *XRD analysis*

XRD analysis of the B-Clay, Y-Clay, G-Clay, and P-Clay (Figs S1–S4, see Supplementary material) and the results of Rietveld refinements are summarized in Table 1. All samples consisted mainly of dioctahedral smectite (montmorillonite), based on the positions of diagnostic diffraction peaks. The largest montmorillonite content was observed for the Y-Clay (98 wt.%). Slightly smaller montmorillonite contents were observed for the G-Clay (88 wt.%) and the B-Clay (83 wt.%), and the P-Clay contained much less montmorillonite (63 wt.%).

Accessory minerals included kaolinite (G-Clay), quartz (Y-Clay, B-Clay, P-Clay, and G-Clay), plagioclase (Y-Clay, B-Clay, and P-Clay), cristobalite (B-Clay and P-Clay), calcite (P-Clay and G-Clay), mordenite (G-Clay), and mica (B-Clay). The montmorillonite 001 reflection ($d_{001}$) was 15.4 Å for the Y-Clay, 15.3 Å for the B-Clay and 15.6 Å for the G-Clay corresponding to a two $H_2O$-layer hydration state of alkaline-earth-smectite consistent with $Ca^{2+}$ as the dominant interlayer cation (Chipera et al., 1997; Ferrage et al., 2005; Goo et al., 2023). The $d_{001}$ value of the P-Clay was ~12.5 Å and is characteristic of Na-montmorillonite hydrated with one $H_2O$ layer (Chipera et al., 1997; Ferrage et al., 2005; Goo et al., 2023).

#### *Chemical composition*

The results of the chemical analysis of the bentonites (Table 2) indicated large amounts of $SiO_2$ (49.24–68.00%) and $Al_2O_3$ (15.59–25.04%) consistent with the presence of major montmorillonite in all samples. CaO varied from 3.09% to 5.17% in the Ca-bentonites (B-Clay, Y-Clay, and G-Clay). CaO in the G-Clay (5.07%) and in the P-Clay (4.39%) originated from montmorillonite but also from calcite that was present as an accessory mineral. MgO varied from 1.31% to 3.19%, consistent with the largely dioctahedral montmorillonite in these samples (Bayram et al., 2010; Lacerda et al., 2023; Shwan et al., 2023). The amounts of $Na_2O$ and $K_2O$ in the B-Clay, Y-Clay, and G-Clay were 0.04–0.28 and 0.18–0.68%, respectively, whereas the P-Clay contained 1.24% of $Na_2O$ and 1.39% of $K_2O$. The amount of $Na_2O$ in Na-montmorillonites generally represented the amount of Na as an exchangeable cation (Lacerda et al., 2023), and the calculated Na content in P-Clay of 0.92% (40 meq 100 $g^{-1}$) was consistent with the amount of Na determined in the exchangeable positions – 39.0 meq 100 $g^{-1}$ (see 'CEC and zeta potential' section below). The loss on ignition (LOI) value originated from $H_2O$ in the interlamellar space and the dehydroxylation of montmorillonite as well as from the de-carbonation of calcite in some samples (P-Clay and G-Clay).

#### *CEC and zeta potential*

The amounts of the exchangeable cations, the total CEC values, and the zeta potential values for bentonites are presented in Table 3.

The total CEC values of bentonites varied from 97 meq 100 $g^{-1}$ (G-Clay) to 120 meq 100 $g^{-1}$ (B-Clay). The dominant cation in

**Table 1.** Quantitative mineralogical composition of bentonites

| Content (wt.%) | B-Clay | Y-Clay | G-Clay | P-Clay |
|---|---|---|---|---|
| Montmorillonite | 83 | 98 | 88 | 63 |
| Kaolinite | — | — | 2 | — |
| Quartz | 3 | 1 | 6 | 2 |
| Plagioclase | 5 | 1 | — | 6 |
| Cristobalite | 7 | — | — | 29 |
| Calcite | — | — | 4 | 1 |
| Mordenite | — | — | 1 | — |
| Mica | 2 | — | — | — |

**Table 2.** Chemical compositions of the bentonites

| Chemical composition (%) | B-Clay | Y-Clay | G-Clay* | P-Clay |
|---|---|---|---|---|
| $SiO_2$ | 64.67 | 57.18 | 49.24 | 68.00 |
| $Al_2O_3$ | 15.59 | 21.03 | 25.04 | 15.99 |
| $Fe_2O_3$ | 3.16 | 4.40 | 5.67 | 1.55 |
| CaO | 5.17 | 3.09 | 5.07 | 4.39 |
| MgO | 1.99 | 3.19 | 1.57 | 1.31 |
| $Na_2O$ | 0.28 | 0.04 | 0.16 | 1.24 |
| $K_2O$ | 0.68 | 0.18 | 0.38 | 1.39 |
| $TiO_2$ | 0.50 | 0.70 | 0.84 | 0.34 |
| LOI | 7.84 | 10.25 | 11.99 | 5.27 |

*Shannon et al. (2017).

https://doi.org/10.1017/cmn.2026.10022 Published online by Cambridge University Press

**Table 3.** Amounts of exchangeable cations, CEC, and zeta (ξ) potential values for bentonites

| | Content (meq 100 $g^{-1}$) | | | | | |
|---|---|---|---|---|---|---|
| | $Ca^{2+}$ | $Mg^{2+}$ | $Na^{+}$ | $K^{+}$ | CEC | ξ potential |
| B-Clay | 99.8 | 17.9 | 1.7 | 1.0 | 120.4 | −21.1 mV |
| Y-Clay | 101.6 | 7.7 | 0.5 | 0.8 | 110.6 | −19.8 mV |
| G-Clay | 67.5 | 26.3 | 1.3 | 1.7 | 96.8 | −15.9 mV |
| P-Clay | 54.9 | 13.5 | 38.5 | 1.8 | 108.7 | −29.0 mV |

exchangeable positions in all three natural bentonites was $Ca^{2+}$, with lesser amounts of $Mg^{2+}$ (8–26 meq 100 $g^{-1}$) and very small amounts of $Na^{+}$ and $K^{+}$. The P-Clay contains mainly $Na^{+}$ (39 meq 100 $g^{-1}$) and $Ca^{2+}$ (55 meq 100 $g^{-1}$) ions in the exchangeable cation positions demonstrating that the P-Clay was a Na/Ca-montmorillonite.

Various data on the electrokinetic properties of montmorillonites have been reported in the literature (Şans et al., 2017; Missana et al., 2018), but generally, the zeta potential of Na-montmorillonites was more negative than the zeta potential of Ca-montmorillonites. For the Ca-montmorillonites studied, the zeta potential varied from −21.1 mV for the B-Clay to −15.9 mV for the G-Clay. As expected, the smallest zeta potential value (−29.0 mV) was observed for the P-Clay, which was a Na/Ca-montmorillonite. These results for Ca-montmorillonites were consistent with the results of Şans et al. (2017). They studied nine different Ca-bentonites with relatively high smectite content in order to relate their zeta potential values to particle size, pH, CEC, smectite structural formula, and layer charge. They reported that negative values of the zeta potential of Ca-bentonites, with smectite contents of between 60 and 95%, varied from −9.5 to −17.4 mV in water at natural pH values. They showed that a negative zeta potential value decreased with increase in CEC for their studied bentonites, although these parameters were not highly correlated. Data for Ca-montmorillonites used in this study revealed an obvious correlation and negative values of zeta potential decreased and became more negative as the CEC values of bentonites increased (B-Clay>Y-Clay>G-Clay).

### *Thermal analysis*

Most clay minerals are thermally characterized by three reactions: (1) processes of dehydration (25–300°C); (2) dehydroxylation (300–700°C); and (3) decomposition/recrystallization (>800°C) (Wolters and Emmerich, 2007; Rehman et al., 2021). The detailed octahedral structure of smectites cannot be determined by XRD analysis, as is possible for more ordered dioctahedral 2:1 phyllosilicates (e.g. illites) (Wolters and Emmerich, 2007). According to Drits et al. (1995), the dehydroxylation behavior of dioctahedral smectites is related to the distribution of cations and vacancies in the octahedral sheet. Depending on the disposition of the OH groups with respect to the vacant octahedral site, two types of configurations in the octahedral sheet of dioctahedral smectites exist: *cis*-vacant and *trans*-vacant. In the *cis*-vacant octahedra, OH groups are located on the same side, whereas in the *trans*-vacant octahedra, they are positioned on the opposite corners of the octahedral site (Drits and Zviagina, 2009; Escamilla-Roa et al., 2014). Thus, an essential characteristic of dioctahedral smectites is the nature of the octahedral vacancy. In general, the dehydroxylation peak temperature obtained by thermal analysis (DTA or differential scanning calorimetry – DSC) can be used for characterization of the structure of the octahedral sheet. *cis*-vacant smectites dehydroxylate at 650–700°C, whereas *trans*-vacant smectites dehydroxylate at 500–550°C. Most montmorillonites exhibit one endothermic dehydroxylation peak near 700°C, and only a few montmorillonites show one endothermic peak near 500°C (Grim and Kulbicki, 1961; Schultz, 1969), whereas other montmorillonites show an endothermic peak doublet between ~500°C and ~700°C (Drits et al., 1995; Emmerich and Kahr, 2001; Wolters and Emmerich, 2007).

The DTA/TG curves of the bentonites investigated are presented in Fig. 2, and mass losses in different temperature regions are presented in Table 4. The DTA curves of the B-Clay, Y-Clay, and G-Clay showed dehydration in the first region, giving rise to an endothermic peak centered at 157°C (B-Clay), 166°C (Y-Clay), and 158°C (G-Clay) with a weak shoulder at 221°C (B-Clay), 230°C (Y-Clay), and 228°C (G-Clay) (Fig. 2a). This endothermic peak with a shoulder was characteristic of Ca-bentonites and corresponds to the evolution of adsorbed $H_2O$ and $H_2O$ coordinated to the interlayer cations. In this region, the TG curves of these bentonites (Fig. 2b) exhibited one dehydration step with a total mass loss of 14.90% (B-Clay), 18.85% (Y-Clay),

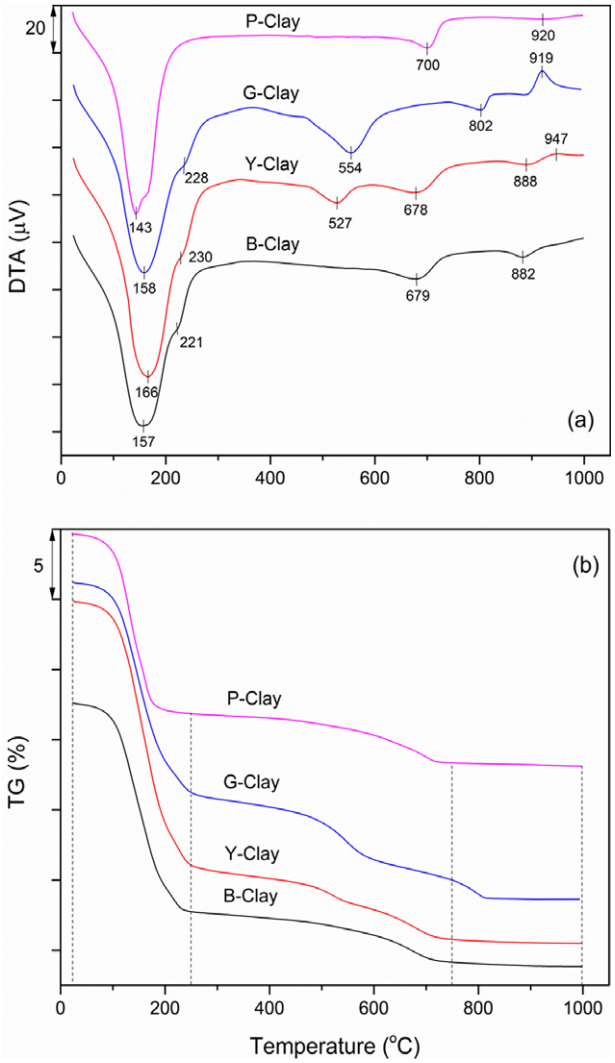



**Figure 2.** Thermal curves of bentonites: (a) DTA and (b) TG.

https://doi.org/10.1017/cmn.2026.10022 Published online by Cambridge University Press

**Table 4.** Mass loss for bentonites over various temperature regions

| | Mass loss (%) from TG curves | | | |
|---|---|---|---|---|
| | 25–250°C | 250–750°C | 750–1000°C | Σ (25–1000)°C |
| B-Clay | 14.90 | 3.81 | 0.30 | 18.81 |
| Y-Clay | 18.85 | 5.31 | 0.28 | 24.44 |
| G-Clay | 15.00 | 6.25 | 1.35 | 22.60 |
| P-Clay | 12.86 | 3.51 | 0.24 | 16.61 |

and 15.00% (G-Clay). For the P-Clay, a single endothermic dehydration peak at 143°C was observed and is characteristic of Na-bentonites (Fig. 2a), with a mass loss from the TG curve of 12.86%. In the dehydroxylation temperature range (250–750°C), DTA curves of B-Clay and P-Clay showed one endothermic peak at 679°C and 700°C, respectively, confirming the predominance of *cis*-vacant octahedra. The endothermic peak for the G-Clay was at 554°C and is characteristic of a *trans*-vacant smectite. The DTA curve for the Y-Clay showed two endotherms at 527°C and 678°C, suggesting that this bentonite possesses both *cis*- and *trans*-vacant octahedra. Drits et al. (1995), Şans et al. (2017), and Zhao et al. (2021) reported that the lower dehydroxylation temperature of *trans*-vacant smectites is caused by the weaker bonds related to the larger number of tetrahedral $Al^{3+}$ cations in the smectite structure. Thermal results in this study were consistent with the chemical analyses (see 'Chemical composition' section below) that confirmed larger amounts of $Al_2O_3$ in the *trans*-vacant smectite (G-Clay) and *cis*-/*trans*-vacant smectite (Y-Clay). The mass loss in the region 250–750°C related to dehydroxylation was 3.81% for the B-Clay and 3.51% for the P-Clay, whereas larger mass losses of 5.31% and 6.25% were observed for the Y-Clay and G-Clay, respectively. The third mass loss for the G-Clay (~1.35%) at temperatures above 750°C, with an endothermic peak at 802°C in the DTA curve, was due to the de-carbonation reaction of calcite present in bentonite (4%, XRD analysis). The P-Clay also contained 1% calcite (XRD analysis), but the endotherm originating from de-carbonation was not apparent in the DTA curve due to overlap with the dehydroxylation peak, which was slightly shifted towards higher temperatures (700°C). Decomposition and recrystallization of the bentonites occurred above 850°C (Wolters and Emmerich, 2007), and occasionally only one of the two reactions was observed in DTA curves. Endotherms were visible at 882°C and 920°C for the B-Clay and P-Clay, respectively, and the G-Clay showed an exotherm at 919°C. In contrast, the Y-Clay showed two peaks: an endotherm at 888°C and an exotherm at 947°C.

### *FT-IR analysis*

Additional structural information about the bentonites was obtained from FT-IR spectra (Fig. 3). The spectral absorption band at 3628 $cm^{-1}$ (Fig. 3a) for all bentonites was attributed to the stretching vibrations of structural OH groups related to various montmorillonite octahedral cations. The broad band at 3434 $cm^{-1}$ originated from OH-stretching vibrations of $H_2O$ in the interlamellar space, together with the bending vibration of $H_2O$ at 1638 $cm^{-1}$. An intense Si-O absorption band at 1039 $cm^{-1}$ was related to the Si–O stretching vibrations in the tetrahedral sheet of montmorillonite, and bands around 525, 469, and 425 $cm^{-1}$ were due to the Al-O-Si, Si-O-Mg, and Si-O-Si bending vibrations, respectively (Zhao et al., 2021). An absorption band corresponding to the Al-Al-OH bending vibrations was observed around 915 $cm^{-1}$ (Fig. 3b) (Danková et al., 2014;

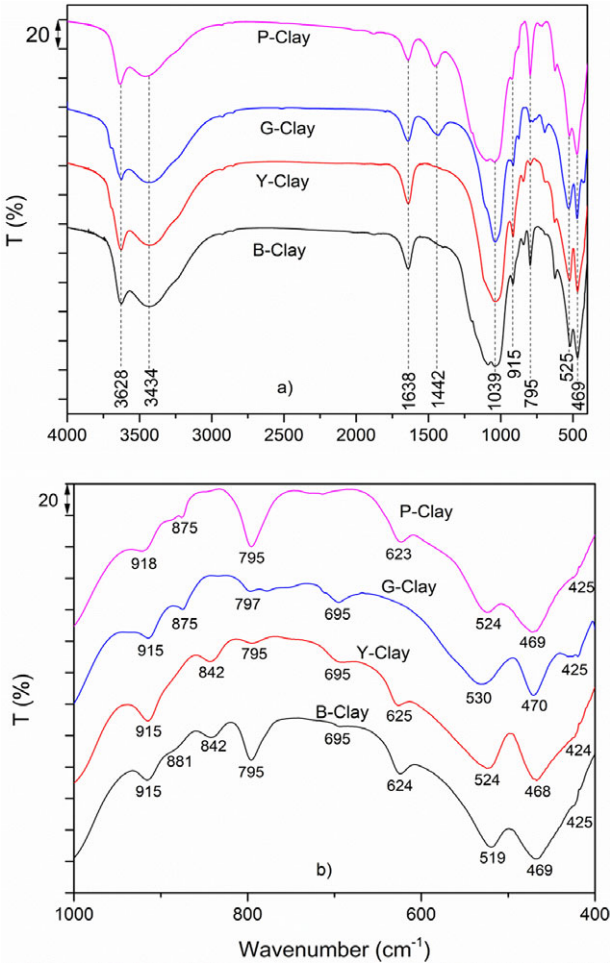



**Figure 3.** FT-IR spectra of bentonites: (a) the 4000–400 $cm^{-1}$ region and (b) the 1000–400 $cm^{-1}$ region.

Zhao et al., 2021; Et-Tayea et al., 2023; Lacerda et al., 2023). An absorption band visible for the B-Clay and Y-Clay at 842 $cm^{-1}$ was related to the Al-Mg-OH bending vibrations consistent with the isomorphic substitution of Al by Mg in the octahedral sheet that is characteristic of some dioctahedral smectites (Lacerda et al., 2023). This band was not visible in spectra of the P-Clay and G-Clay probably because it was overlapped with the band at 875 $cm^{-1}$ originating from calcite. The presence of calcite in these bentonites was also confirmed by the presence of a band at 1442 $cm^{-1}$ (Fig. 3a) (Rehman et al., 2021; Shwan et al., 2023). The high-intensity band at 795 $cm^{-1}$ visible for the B-Clay and P-Clay was due to the Si-O stretching vibration, confirming the presence of cristobalite (Qiao et al., 2019), and the low-intensity band around 796 $cm^{-1}$ for the G-Clay and Y-Clay confirmed the presence of quartz (Et-Tayea et al., 2023). A band visible at 695 $cm^{-1}$ for the B-Clay, Y-Clay, and G-Clay was ascribed to the quartz impurity. A weak shoulder at ~3690 $cm^{-1}$ visible in FT-IR spectra of the G-Clay and Y-Clay originated from the presence of traces of kaolinite (Belousov et al., 2021; Zhao et al., 2021).

The bentonites (especially G-Clay and Y-Clay) contained $Fe_2O_3$, but bands related to Fe-Al-OH and Fe-Fe-OH vibrations (881 and 818 $cm^{-1}$) were absent from their FT-IR spectra, with the exception of the B-Clay where a small shoulder was visible at 881 $cm^{-1}$. The band at ~624 $cm^{-1}$ in the FT-IR spectra of the B-Clay, Y-Clay, and P-Clay was assigned to coupled Al-O and Si-O out-of-plane

https://doi.org/10.1017/cmn.2026.10022 Published online by Cambridge University Press

vibrations. The position of this band may be related to the structure of the octahedral sheet, specifically to the type of octahedral vacancy, and can be correlated to the dehydroxylation peak temperature on DTA curves. Belousov et al. (2021) reported FT-IR and DTA analysis of an industrial bentonite IB-6. They observed a FT-IR band near 622 $cm^{-1}$, which they attributed to the coupled Al-O and Si-O out-of-plane vibrations. The DTA curve of IB-6 showed an endothermic dehydroxylation peak at 667°C, indicating the predominance of *cis*-vacant octahedra. In another study by Musso et al. (2022), FT-IR spectra of selected (red and gray) bentonites showed a band near 620 $cm^{-1}$ due to coupled Al-O out-of-plane and Si-O vibrations, characteristic of montmorillonite. Their DTA curves showed endothermic dehydroxylation peaks at 620°C with a mass loss up to 4.0% in the range 200–720°C, indicating that these smectites were more similar to *cis*-vacant variants. Overall, the FT-IR results reported in this study were in accordance with the results of the XRD analysis (see 'XRD analysis' section below).

### *Textural properties*

The $N_2$ adsorption-desorption isotherms of B-Clay, Y-Clay, G-Clay, and P-Clay (Figs S5 and S6; see Supplementary material) had a common shape similar to data in numerous publications (Kaufhold et al., 2013; Jabłońska et al., 2019; Mannu et al., 2019). The adsorption portion of the isotherms consisted of a vertical, clearly visible, increase in the volume of adsorbed $N_2$ in the region $p/p_0 \leq 0.05$, with a transition to a moderate, almost-linear increase lasting up to $p/p_0=0.7$, followed by a sharp increase in the adsorbed volume of $N_2$ in the region of high $p/p_0$.

The first portion of the isotherm corresponded to adsorption of $N_2$ in the microporous region with simultaneous adsorption on the outer surfaces of particles, whereas the further slow growth was exclusively related to adsorption of $N_2$ in the monolayer. By increasing the relative pressure, $N_2$ was packed uniformly in the second adsorption layer, and with a further increase in $p/p_0$, adsorption occurred in the following layers. Depending on the textural properties of the material, two resulting isotherm shapes were possible with further increase in $p/p_0$. For mesoporous materials, capillary condensation occurred as a result of the complete filling of the available mesopore space. In the second case, for non-porous and macroporous materials, the conditions for multi-layer adsorption were achieved at high $p/p_0$ values, and the delayed capillary condensation occurred on the surface of the particles. For mesoporous materials (type IV isotherm according to IUPAC nomenclature), the completion of mesopore filling was recognizable by the appearance of a plateau on the adsorption isotherm, as well as on its corresponding desorption branch, in the region of high relative pressures. The plateau on the isotherms is not visible in the majority of literature data for untreated bentonites (Sing and Williams, 2004). In fact, a sharp increase in the amount of adsorbed $N_2$ is an indicator of $N_2$ condensation in the interparticle space, on the surface of particles, and/or condensation in macropores. Despite the existence of a hysteresis loop (clearly visible in most published works), which is also a common feature of the isotherms for the bentonites studied here, the isotherms can be classified as type II according to the IUPAC nomenclature (Thommes et al., 2015) or IIb according to Rouquerol et al. (1999). The isotherms of B-Clay and P-Clay were similar (IIb type) (Fig. S5; see Supplementary material), and resultant textural parameters (Table 5) were similar (especially values of $V_{mic}$, $V_{mes}$, and $V_{tot}$). The IIb isotherm form was attributed to adsorption on aggregates of plate-like particles which, therefore, possessed non-rigid groove- and/or slit-shaped pores (Rouquerol et al., 1999).

**Table 5.** Textural properties of bentonites

| | B-Clay | Y-Clay | G-Clay | P-Clay |
|---|---|---|---|---|
| Specific surface area ($SSA_{N2BET}$) ($m^2\ g^{-1}$) | 63 | 105 | 88 | 57 |
| Micropore volume ($V_{mic}$) ($cm^3\ g^{-1}$) | 0.025 | 0.043 | 0.035 | 0.024 |
| Mesopores volume ($V_{mes}$) ($cm^3\ g^{-1}$) | 0.137 | 0.114 | 0.084 | 0.152 |
| Pore volume ($V_{tot}$) ($cm^3\ g^{-1}$) | 0.192 | 0.160 | 0.127 | 0.199 |
| Average pore diameter ($D_p$) (nm) | 8.7 | 4.3 | 3.8 | 10.7 |

The $SSA_{N2BET}$ of the studied samples decreased in the following order: Y-Clay>G-Clay>B-Clay>P-Clay, and the $SSA_{N2BET}$ of the P-Clay was only slightly lower than that of the B-Clay (57 $m^2\ g^{-1}$ *vs* 63 $m^2\ g^{-1}$). As Na-bentonites usually show $SSA_{N2BET}$ values ≤40 $m^2\ g^{-1}$ (Kaufhold et al., 2010), the P-Clay appears more similar to a Na/Ca-montmorillonite. The largest $SSA_{N2BET}$ value was obtained for the Y-Clay (105 $m^2\ g^{-1}$), and the $SSA_{N2BET}$ of the G-Clay was slightly lower (88 $m^2\ g^{-1}$). Such high values of $SSA_{N2BET}$ were not unexpected for Ca-bentonites with a large montmorillonite content, as $Ca^{2+}/Mg^{2+}$ bentonites (<5% $Na^+$) in particular show a broad distribution of $SSA_{N2BET}$ values in the range 50–130 $m^2\ g^{-1}$ (Kaufhold et al., 2010; Kaufhold et al., 2013). Reported $SSA_{N2BET}$ values were consistent with the results of chemical analyses, CEC, and zeta potential (see 'Chemical composition' and 'CEC and zeta potential' sections below). However, it is important to note that the shape of the isotherms and these SSA $_{N2BET}$ values were not only a consequence of the content of montmorillonite, but also of the overall mineralogical and chemical composition and particle size of the bulk clay and even of the pre-treatment preparation procedures used before measurement (Noyan et al., 2006). Therefore, the almost uniform mineralogical composition (98% montmorillonite) of the Y-Clay was an exception, evidenced by the unique hysteresis loop almost parallel to the $p/p_0$ axis, and significantly wider than the loops of the remaining three samples, closely resembling the H4 type that occurs in slit-shaped micropore materials.

## *Adsorption of aflatoxin B1 by bentonites*

Adsorption of AFB1 (%) *versus* amount of adsorbent, from 0.002 to 0.02% (w/v) for B-Clay, Y-Clay, G-Clay, and P-Clay, at pH 3 and 7, is presented in Table 6. Experiments performed according to the Commission Implementing Regulation (EU) showed that at pH 5 all studied bentonites were highly efficient at adsorbing AFB1 (adsorption index >90%) (Table 6).

Data measured at pH 3 and 7 (Table 6) illustrated that the percentage of AFB1 adsorption by bentonites increased with an increasing amount of each adsorbent in suspension. At the largest amount (0.02% w/v), adsorption of AFB1 by all bentonites was very high (>90%) with no differences in their adsorption at pH 3 and 7. With a decrease in the amount of bentonite, the differences in AFB1 adsorption became more apparent. For the smallest amount (0.002% w/v), for the Y-Clay and G-Clay, adsorption of AFB1 was slightly higher at pH 3 (50.1% for Y-Clay and 45.6% for G-Clay) than at pH 7 (42.4% for Y-Clay and 30.9% for G-Clay). For the other two clays, AFB1 adsorption was practically independent of pH, but was much higher for the B-Clay (Ca-dominant, *cis*-vacant montmorillonite), 52.2% at pH 3 and 50.0% at pH 7, than for the P-Clay (Na/Ca form, *cis*-vacant montmorillonite), 31.1% at pH 3 and 28.9% at pH 7.

https://doi.org/10.1017/cmn.2026.10022 Published online by Cambridge University Press

**Table 6.** Adsorption of AFB1 ($C_0$=4 ppm) by bentonites at pH 3, 5, and 7

| Amount of bentonite (% w/v) | AFB1 adsorption (%) | | |
|---|---|---|---|
| | pH 5 | pH 3 | pH 7 |
| **B-Clay** | | | |
| 0.02 | 98.0 | 99.1 | 97.9 |
| 0.01 | | 98.1 | 93.5 |
| 0.005 | | 88.4 | 82.4 |
| 0.002 | | 52.2 | 50.0 |
| **Y-Clay** | | | |
| 0.02 | 97.6 | 97.8 | 97.4 |
| 0.01 | | 95.6 | 89.3 |
| 0.005 | | 86.4 | 75.4 |
| 0.002 | | 50.1 | 42.4 |
| **G-Clay** | | | |
| 0.02 | 92.3 | 91.6* | 91.9 |
| 0.01 | | 89.5* | 78.6 |
| 0.005 | | 71.5* | 58.0 |
| 0.002 | | 45.6* | 30.9 |
| **P-Clay** | | | |
| 0.02 | 91.7 | 93.5 | 90.8 |
| 0.01 | | 83.8 | 76.9 |
| 0.005 | | 62.5 | 55.4 |
| 0.002 | | 31.1 | 28.9 |

*Shannon et al. (2017).

Adsorption of AFB1 by bentonites was further investigated through the evaluation of adsorption isotherms, measured in phosphate buffer, at pH 3 and 7, and results are presented in Fig. 4. Generally, the isotherms were obtained by plotting the amounts of solute adsorbed per unit weight of adsorbent (mg $g^{-1}$) against the equilibrium concentrations of the solute in the solution (mg $L^{-1}$). The results showed that at both pH values, non-linear adsorption isotherms were obtained for all bentonites, and adsorption of AFB1 increased as the initial toxin concentration increased, with the greater adsorption observed at pH 3. Non-linear adsorption isotherms suggested a complex AFB1 adsorption mechanism. The experimental data were fitted by common non-linear Langmuir (Eqn (1)) and Freundlich (Eqn (2)) models for the adsorption of AFB1 on all bentonites:

$$q_e = \frac{q_m K_L c_e}{1 + K_L c_e} \quad (1)$$

$$q_e = K_F c_e^{\frac{1}{n}} \quad (2)$$

where $c_e$ (mg $L^{-1}$) is the concentration of AFB1 in solution at equilibrium, $q_e$ (mg $g^{-1}$) is the amount of AFB1 adsorbed by each bentonite at equilibrium, $q_m$ (mg $g^{-1}$) is the maximum amount of AFB1 adsorbed by the bentonites, $K_L$ (L $mg^{-1}$) and $K_F$ ($L^n mg^{1-n} g^{-1}$) are the Langmuir and Freundlich constants, respectively, and $1/n$ is a heterogeneity factor (dimensionless). The Langmuir theoretical isotherm model predicts monolayer adsorption at specific active sites on a homogeneous adsorbent surface, meaning that no

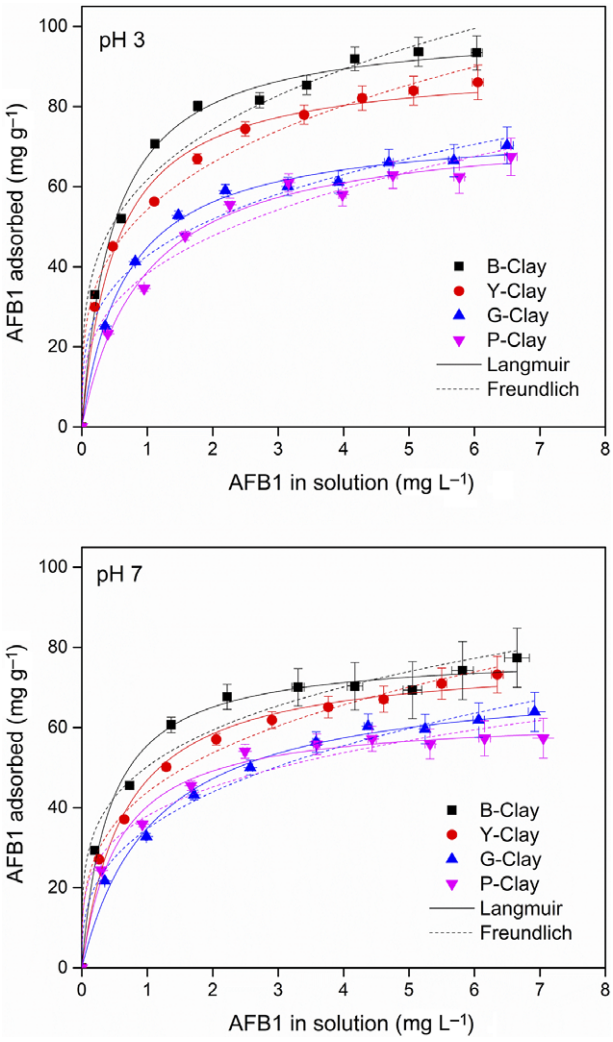



**Figure 4.** Adsorption isotherms for AFB1 adsorption by bentonites: Langmuir model (continuous line) and Freundlich model (dashed line).

further adsorption occurs once an adsorbate is adsorbed at these sites in the adsorbent. The Freundlich model usually considers a multi-layer adsorption process on the heterogeneous surface or surface supporting sites of various affinities. This means that the adsorption process is not restricted to the formation of a single adsorbate layer on the adsorbent surface (Wang et al., 2018). Parameters of Langmuir and Freundlich isotherms are listed in Table 7.

The $R^2$ (coefficient of determination) shown in Table 7 suggested that the isotherms are empirically consistent with both the Langmuir and Freundlich models, with slightly larger values observed for the Langmuir model. The calculated maximum adsorption capacities ($q_m$) for AFB1 derived from Langmuir plots of the isotherms were from 0.24 mol $kg^{-1}$ (75.43 mg $g^{-1}$) at pH 3 and 0.20 mol $kg^{-1}$ (62.91 mg $g^{-1}$) at pH 7 for the P-Clay to 0.32 mol $kg^{-1}$ (100.25 mg $g^{-1}$) at pH 3 and 0.25 mol $kg^{-1}$ (78.58 mg $g^{-1}$) at pH 7 for the B-Clay (Table 7).

The value of the $1/n$ dimensionless parameter from the Freundlich model (Table 7) is usually used to determine the adsorption affinity of the adsorbate to adsorb on various adsorbents. Depending on the value $1/n$, the isotherm can be of S-type ($1/n>1$), C-type ($1/n=1$), or L-type ($0<1/n<1$). An S-type

https://doi.org/10.1017/cmn.2026.10022 Published online by Cambridge University Press

**Table 7.** Characteristic parameters of AFB1 adsorption isotherms

| | Langmuir | | | | | |
|---|---|---|---|---|---|---|
| | pH 3 | | | pH 7 | | |
| | $q_m$ (mg g$^{-1}$) | $K_L$ (L mg$^{-1}$) | $R^2$ | $q_m$ (mg g$^{-1}$) | $K_L$ (L mg$^{-1}$) | $R^2$ |
| B-Clay | 100.25 | 2.060 | 0.993 | 78.58 | 2.410 | 0.987 |
| Y-Clay | 90.73 | 1.916 | 0.988 | 77.46 | 1.534 | 0.989 |
| G-Clay | 75.00 | 1.488 | 0.994 | 73.16 | 0.910 | 0.992 |
| P-Clay | 75.43 | 1.054 | 0.989 | 62.91 | 1.785 | 0.989 |
| | Freundlich | | | | | |
| | pH 3 | | | pH 7 | | |
| | $1/n$ | $K_F$ ($L^n$ mg$^{1-n}$ g$^{-1}$) | $R^2$ | $1/n$ | $K_F$ ($L^n$ mg$^{1-n}$ g$^{-1}$) | $R^2$ |
| B-Clay | 0.266 | 61.766 | 0.968 | 0.240 | 50.250 | 0.962 |
| Y-Clay | 0.282 | 54.284 | 0.986 | 0.291 | 43.828 | 0.989 |
| G-Clay | 0.280 | 42.746 | 0.966 | 0.337 | 34.745 | 0.985 |
| P-Clay | 0.317 | 38.263 | 0.961 | 0.250 | 37.947 | 0.958 |

isotherm indicates weak adsorption between the adsorbate and adsorbent, a C-type means that the adsorption is linear, and an L-type isotherm suggests that the interactions between adsorbate and adsorbent are strong (Wang et al., 2018). Calculated $1/n$ values in the range 0.266–0.317 at pH 3 and 0.240–0.337 at pH 7 were characteristic of an L-type isotherm, demonstrating strong binding of AFB1 to all bentonites at both pH values.

The Gibbs free energy ($\Delta G$) can be estimated from the Langmuir adsorption constant (Milonjić, 2007):

$$\Delta G = -RT\ln K_L * \quad (3)$$

$$K_L^* = K_L M(\mathrm{AFB1}) C(H_2O) \quad (4)$$

where $T$ is the absolute temperature in K, and R is the universal gas constant (8.314 J mol$^{-1}$ K$^{-1}$). The dimensionless Langmuir sorption constant $K_L$* was derived from the Langmuir adsorption constant $K_L$ (L mg$^{-1}$), where $M$ (AFB1 ) is the molar mass of AFB1 (312,277 mg mol$^{-1}$) and $C(H_2O)$ is the molar concentration of water (55.56 mol dm$^{-3}$). The results are presented in Table 8. Calculated $\Delta G$ values for all bentonites were negative and similar, indicating that the AFB1 adsorption process was spontaneous in nature at both pH values.

Non-linear isotherms and high adsorption of AFB1 by various bentonites were reported by many authors, but depending on the characteristics of the bentonites as well as experimental conditions described in these papers, AFB1 adsorption capacities differed significantly. For example, Gan et al. (2019) measured AFB1 adsorption isotherms for six Ca saturated smectite samples in water, following the procedure of Grant and Phillips (1998) at 25°C for 24 h, showing substantial differences in AFB1 affinity and adsorption capacity. They noticed that compared with Na-saturation, Ca-saturation improved the AFB1 adsorption capacities of all six samples, confirming observations that Ca-bentonites were in general better AFB1 adsorbents than Na-bentonites. Marroquín-Cardona et al. (2009, 2022) reported non-linear (Langmuir) isotherms for adsorption of AFB1 by Na-bentonite in ultra-pure water (UP-$H_2O$) by adjusting the pH to 2 or 6.5 (with HCl or NaOH). Adsorption of AFB1 was followed by various initial toxin concentrations ranging from 0.4 to 8 μg mL$^{-1}$ in 5 mL of solution and with 0.1 mg of adsorbent, with a contact time of 2 h. They reported favorable AFB1 adsorption at both pH values, with slightly less adsorption observed at pH 2. Vekiru et al. (2015) performed isotherm experiments for AFB1 adsorption by seven bentonites: dioctahedral smectites (two *cis*-vacant Ca-smectites: R and M34; four *cis*-vacant Na-smectites: MB, B7, M5, and M32; and one *trans*-vacant Na-smectite: C2) in phosphate buffer (potassium di-hydrogen phosphate/sodium hydrogen phosphate-dihydrate) at pH 7 (Vekiru et al., 2007), using the procedure of Grant and Phillips (1998). The largest AFB1 capacity was found for *cis*-vacant Na-smectite (MB, 0.44 mol kg$^{-1}$) and the smallest was for *trans*-vacant Na-smectite (C2, 0.26 mol kg$^{-1}$). D'Ascanio et al. (2019) reported AFB1 adsorption isotherms for 29 dioctahedral smectite (bentonite) samples, measured at 37°C, pH 7 (phosphate buffer: potassium di-hydrogen phosphate 2-hydrate/di-sodium hydrogen phosphate 12-hydrate) and at contact time of 90 min. They obtained non-linear (Langmuir) isotherms for all bentonites studied and found that Na-bentonites exhibited maximum AFB1 adsorbed amounts >100 μg mg$^{-1}$ (0.32 mol kg$^{-1}$), compared with much smaller amounts measured with Ca-bentonites.

The data above illustrated that it is difficult to compare results from this study with literature data because the majority of investigations were performed either in distilled water (with or without adjustment of pH) or using different salts/acids for preparation of buffers at acidic (acetate, citrate, or phosphate salts) and at neutral (mainly phosphate salts) pH values. Also, in literature studies, experiments were performed with different initial AFB1 concentrations, at different contact times or at different temperatures. However, similar to results obtained in this study, several studies showed that the differences in AFB1 adsorption by bentonites at different pH values were clearly visible, illustrating the importance of solution pH in toxin adsorption.

Despite the abundance of literature data on the adsorption of AFB1 by bentonites in aqueous solutions, there is still a lack of information on the effects of buffer-solution compositions on the montmorillonite surface structure and its properties and consequently on AFB1 adsorption. Clay minerals are well known to be common cation exchangers, and thus when montmorillonite is suspended in an electrolyte solution, a significant fraction of exchangeable cations in the montmorillonite interlayer or from the surface appears in the solution and may be replaced by hydrogen ions or other cations from a buffer solution (Nagy et al., 1997). For these reasons, the behavior of bentonites in buffer solutions (pH 3 and 7) with and without the presence of AFB1 was investigated. For comparison, the behavior of bentonites with or without AFB1 in water without adjustment of pH was also studied under the same conditions. After separation of phases, supernatants were collected and the amounts of exchangeable

**Table 8.** Gibbs free energy for AFB1 adsorption by bentonites

| | $\Delta G$ (kJ mol$^{-1}$) | |
|---|---|---|
| | pH 3 | pH 7 |
| Y-Clay | –41.5 | –42.8 |
| G-Clay | –42.9 | –42.4 |
| B-Clay | –43.1 | –43.5 |
| P-Clay | –42.3 | –41.1 |

https://doi.org/10.1017/cmn.2026.10022 Published online by Cambridge University Press

cations ($Ca^{2+}$, $Mg^{2+}$, and $Na^{+}$) released from montmorillonites were determined. Possible dissolution of Si and Al from the tetrahedral and octahedral sheets was also measured. The amounts of cations released were compared with the amounts of exchangeable cations in each bentonite (Table 3) calculated in mol $kg^{-1}$ and with maximum experimentally adsorbed amounts of AFB1 (mol $kg^{-1}$). The results are presented in Fig. 5.

The results in Fig. 5b showed that negligible amounts of $Ca^{2+}$, $Mg^{2+}$, and $Na^{+}$ were detected in the aqueous solution without buffer for the B-Clay, Y-Clay, and G-Clay. However, significant amounts

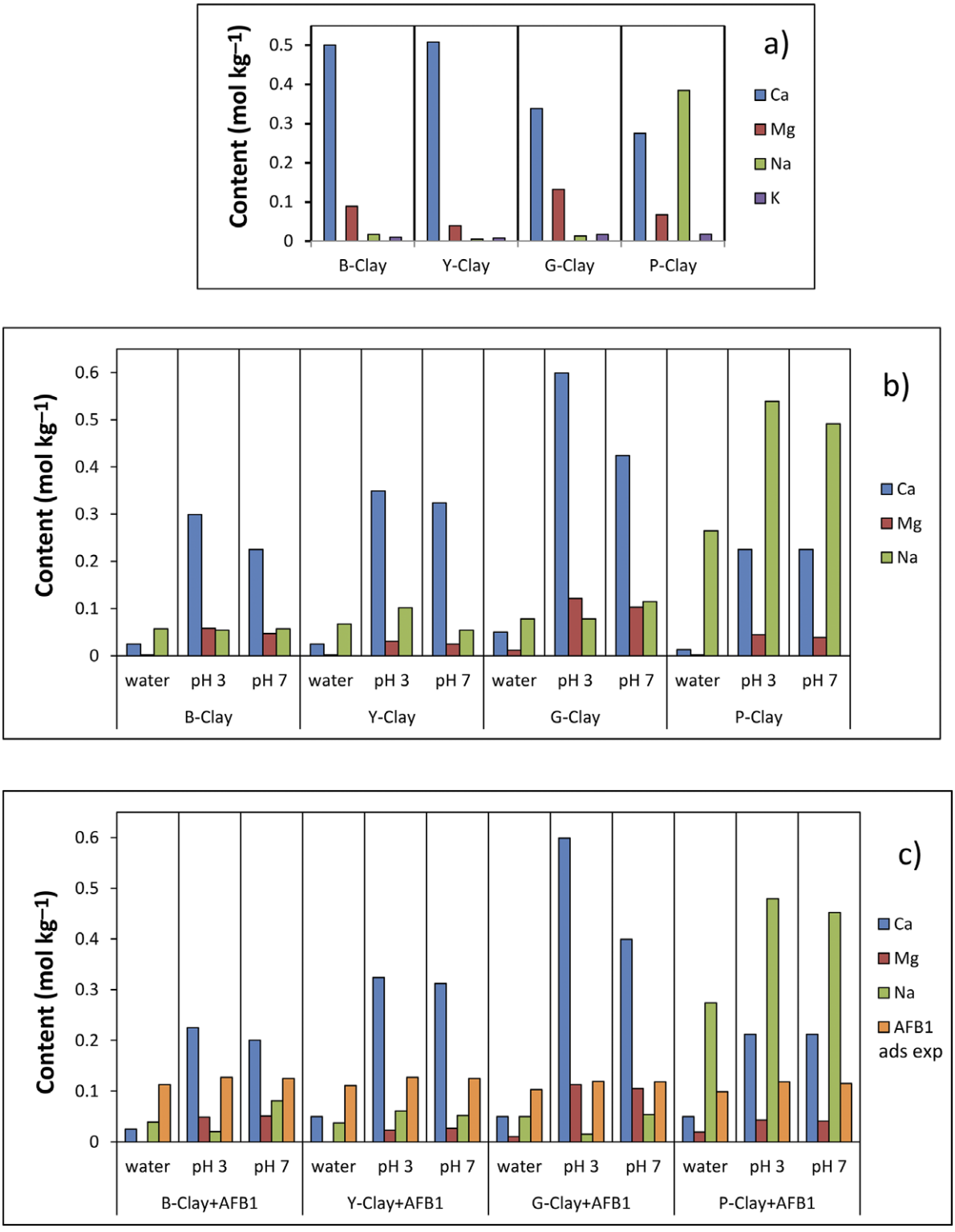



**Figure 5.** Cations in bentonites: (a) amounts of exchangeable cations; (b) amounts of cations released in water and buffer solutions; and (c) amounts of cations released in water and buffer solutions in the presence of AFB1.

https://doi.org/10.1017/cmn.2026.10022 Published online by Cambridge University Press

of $Ca^{2+}$ and $Mg^{2+}$ were released from all of the bentonites studied into the buffer solutions at pH 3 or 7. This behavior in buffer solutions was in agreement with the results of Metz et al. (2005) and was attributed mainly to cation exchange. In the phosphate buffer used in the present study, at pH 3, $K^+$, $H^+$, $H_2PO_4^-$, and $H_3PO_4^-$ were the dominant species in solution (Tanyol et al., 2015), and the results suggested that large amounts of $Ca^{2+}$ and $Mg^{2+}$ from the montmorillonite interlayers and surfaces were replaced by $K^+$ and $H^+$ from the buffer solution. The larger amount of $Ca^{2+}$ dissolved in the phosphate buffer at pH 3 than the amount in exchange sites for the G-Clay probably resulted from dissolution of accessory calcite that makes up 4% of this bentonite (see 'XRD analysis' section below) (Hofmann et al., 2004). At pH 7, $K^+$, $HPO_4^{2-}$, and $H_2PO_4^-$ ions were mainly present in the buffer solution (Tanyol et al., 2015), and the presence of $K^+$ induced similar behavior as at pH 3, reflecting exchange of $Ca^{2+}$ and $Mg^{2+}$ from interlayer and surface sites with $K^+$ ions. The behavior of divalent cations in the buffer at pH 3 and 7 was thus expected and could be explained by their properties shown in Table 9 (Marcus, 1991). $Ca^{2+}$ has a larger ionic radius and a smaller hydrated radius than $Mg^{2+}$, meaning that $Ca^{2+}$ can be exchanged easily with $K^+$ with the smallest hydrated radius in the buffer solution. Although an $H^+$ ion has the smallest ionic radius, it also has a large hydrated radius and can replace some cations from the interlayer space of montmorillonites and at their external surfaces. It can also lead to protonation of edge groups forming -Si-OH groups at tetrahedral sheet edges or -Al-$OH_2$ groups at octahedral sheet edges at pH 3 (Wang et al., 2010).

For the P-Clay (Na/Ca-montmorillonite), a similar trend for the release of Ca and Mg in buffers (pH 3 and 7) and in water was observed as for the B-Clay, Y-Clay, and G-Clay. However, for the P-Clay, a large amount of Na was detected in the water as well as in the buffer solution at pH 3 and 7 compared with its amount in exchange sites. Similar behavior of Na-bentonite in water was noted by Marroquín-Cardona et al. (2022), who reported a large amount of Na released in the water, 0.32 mol $kg^{-1}$, compared with the amount in exchange sites (0.59 mol $kg^{-1}$), whereas only small amounts of Ca and Mg were found in water solution (0.03 and 0.02 mol $kg^{-1}$) compared with their amounts in the exchange sites (0.33 and 0.20 mol $kg^{-1}$). In this study, the large amount of Na in the distilled water experiment suggested that the commercial P-Clay had been Na saturated but was insufficiently washed (chloride anions were detected by energy dispersive X-ray spectroscopy (EDS) analysis, results not shown). The large amount of Na released into solution at pH 3 and 7 confirmed its exchange with cations from the buffer solutions. The results for all bentonites confirmed that exchange was marked by the notable substitution of preferably divalent $Ca^{2+}$ and $Mg^{2+}$ with $K^+$ and/or $H^+$ derived from buffers. Additionally, the presence of negligible amounts of Al and Si in buffer solutions (pH 3 and 7) for all bentonites indicated that dissolution of montmorillonites or accessory mineral phases (aluminosilicates and amorphous $SiO_2$ phases) did not occur (Hofmann et al., 2004; Metz et al., 2005).

**Table 9.** Properties of cations

| Cation | $r$ (nm)[a] | $\Delta r$ (nm)[a] | $n$[a] | $\Delta G$ (kJ $mol^{-1}$)[a] |
|---|---|---|---|---|
| $H^+$ | 0.030 | 0.300 | 12.0 | –1050 |
| $Ca^{2+}$ | 0.100 | 0.171 | 7.2 | –1505 |
| $Mg^{2+}$ | 0.072 | 0.227 | 10.0 | –1830 |
| $Na^+$ | 0.102 | 0.116 | 3.5 | –365 |
| $K^+$ | 0.138 | 0.074 | 2.6 | –295 |

$r$, ionic radius; $\Delta r$, width of hydration shell; $n$, number of water molecules in this shell; $\Delta G$, molar Gibbs energy of hydration; [a]Marcus (1991).

Compared with observed behavior of bentonites in buffer solutions at pH 3 and 7 (Fig. 5b), only slightly smaller amounts of $Ca^{2+}$ and $Mg^{2+}$ released were observed in the presence of AFB1 (Fig. 5c). These results suggested that when AFB1 was present in buffer solutions, AFB1 adsorption occurred simultaneously with ion exchange of native cations from the interlayer of montmorillonites and at their surfaces with ions from buffers. Negligible amounts of Al and Si were detected in supernatants of all bentonites in the presence of AFB1.

The dominant interlayer cations in the B-Clay, Y-Clay, and G-Clay are $Ca^{2+}$ and $Mg^{2+}$; thus, comparison of the amounts of divalent cations that were not released into the buffer solution in the presence of AFB1 with the amount of adsorbed AFB1 by each bentonite supported the suggestion that these divalent cations were the active sites at which toxin was adsorbed. Therefore, although significant amounts of divalent cations were released into the buffer solutions being exchanged with $K^+$ (pH 3 and 7) and $H^+$ (pH 3), the montmorillonite in bentonites still contained large amounts of divalent active sites available for AFB1 adsorption. Additionally, because $Ca^{2+}$ and $Mg^{2+}$ ions were replaced simultaneously with $K^+$ and/or $H^+$ from buffer solutions during AFB1 adsorption by bentonites, with an increase in the initial AFB1 concentration (isotherm study) and saturation of divalent active sites, the adsorbed monovalent cations also became active sites for AFB1 adsorption. Less and similar adsorption of AFB1 by all bentonites at pH 7, observed at greater initial AFB1 concentrations (Fig. 4b), may be explained by a lower proton concentration in buffer solution. In addition, similar to the behavior of bentonites in water, negligible amounts of $Ca^{2+}$, $Mg^{2+}$, and $Na^+$ were detected in the aqueous solution in the presence of AFB1 for the B-Clay, Y-Clay, and G-Clay and maximum adsorbed amounts of AFB1 were similar to the amounts of toxin adsorbed in both buffers (Fig. 5a). Thus, because AFB1 adsorption by these bentonites in buffer solutions occurred simultaneously with ion exchange, both divalent and monovalent cations were the sites at which AFB1 was adsorbed. In contrast, in pure water solution where ion exchange did not occur, the dominant divalent cations in interlayers and at surfaces were involved in the AFB1 adsorption process.

The non-linear isotherms reported in this study revealed a complex AFB1 adsorption mechanism that probably results from a combination of several different interactions between the AFB1 molecule and montmorillonite. Deng et al. (2010) proposed that the AFB1 molecule occupied the interlayer space of montmorillonite together with exchangeable cations and $H_2O$ molecules, and that toxin adsorption occurred via H-bonding between the carbonyl oxygens and the hydration-shell of interlayer cations. In the case of H-bonding through $H_2O$ bridges in solution, the cations would not affect the AFB1/montmorillonite bond strength. Deng et al. (2010) also reported that the size and valence of cations as well as the presence of unpaired electrons in d-orbitals may influence the adsorption of AFB1. Daković et al. (2008, 2012) studied the <5 μm fraction of the G-Clay as well as its Cu- and Zn-modified forms as AFB1 adsorbents in buffer solution at pH 3. In both studies, adsorption of AFB1 was greater by the Cu- and Zn-modified <5 μm fraction of the G-Clay than by the starting material. Daković et al. (2008) reported that in the Cu-modified <5 μm fraction of the G-Clay, the primary interlayer cations were Ca and Cu, and the

https://doi.org/10.1017/cmn.2026.10022 Published online by Cambridge University Press

presence of Cu enhanced AFB1 adsorption. For the Zn-modified <5 μm fraction of the G-Clay, greater AFB1 adsorption appeared to result in the formation of chelation complexes between Ca, Mg, and Zn and AFB1 molecules. The authors interpreted adsorption in terms of the radii of the exchangeable cations, increasing in the order: Mg<Zn<Ca. Although Zn has a larger ionic radius than Mg, it can interact more strongly with AFB1 than Mg because of the presence of d-electrons (Daković et al., 2012). All of these observations showed that the properties of exchangeable cations, particularly their size, charge, and the presence/absence of d-electrons, play a major role in AFB1 adsorption by montmorillonite at pH 3 and 7.

The cation properties presented in Table 9 (Marcus, 1991) suggested that because $Mg^{2+}$ has the largest hydrated radius, it was expected to be the primary adsorption site in the bentonites studied for AFB1 molecules, followed by $Ca^{2+}$. When these adsorption sites were fully occupied with AFB1 molecules, AFB1 adsorption continued via interactions with monovalent cations ($Na^+$ and $K^+$). In addition, protonated edge groups existing at pH 3 in tetrahedral or octahedral sheets, as well as protons at the surfaces or in the interlayers of montmorillonites, created new active sites that enhance AFB1 adsorption. Overall, irrespective of whether Na- or Ca-bentonites are better AFB1 adsorbents, the data from the present study suggest that all exchangeable cations present in the interlayer and at the surface as well as edge groups of montmorillonite were involved in AFB1 adsorption. The affinity of exchangeable cations toward AFB1 increased in the following order: $K^+<Na^+<Ca^{2+}<Mg^{2+}$.

In addition to the effects of exchangeable cation on AFB1 adsorption, a variety of other factors (mineralogical, structural, chemical, and physico-chemical characteristics of smectite) influenced adsorption. Generally, greater AFB1 adsorption was achieved with Ca-bentonites (B-Clay: *cis*-vacant; Y-Clay: *cis/trans*-vacant; and G-Clay: *trans*-vacant), and the AFB1 adsorption capacity increased with an increase in the CEC of these montmorillonites, which contrasts with the conclusions of Deng et al. (2012). The P-Clay (*cis*-vacant montmorillonite containing $Na^+$ and $Ca^{2+}$ as primary cations in the interlayer and at the surface) exhibited the lowest AFB1 adsorption capacity at both pH values probably due to its having the smallest montmorillonite content (63%). However, at pH 3, the AFB1 capacity of this clay was similar to that of the G-Clay (*trans*-vacant, 88% of montmorillonite) in which $Ca^{2+}$ was the dominant interlayer cation. Although literature data would suggest that the *trans*-vacant G-Clay would have a lower AFB1 adsorption capacity (Vekiru et al., 2015), the G-Clay exhibited a much greater AFB1 capacity at pH 7 than the P-Clay, probably due to its larger

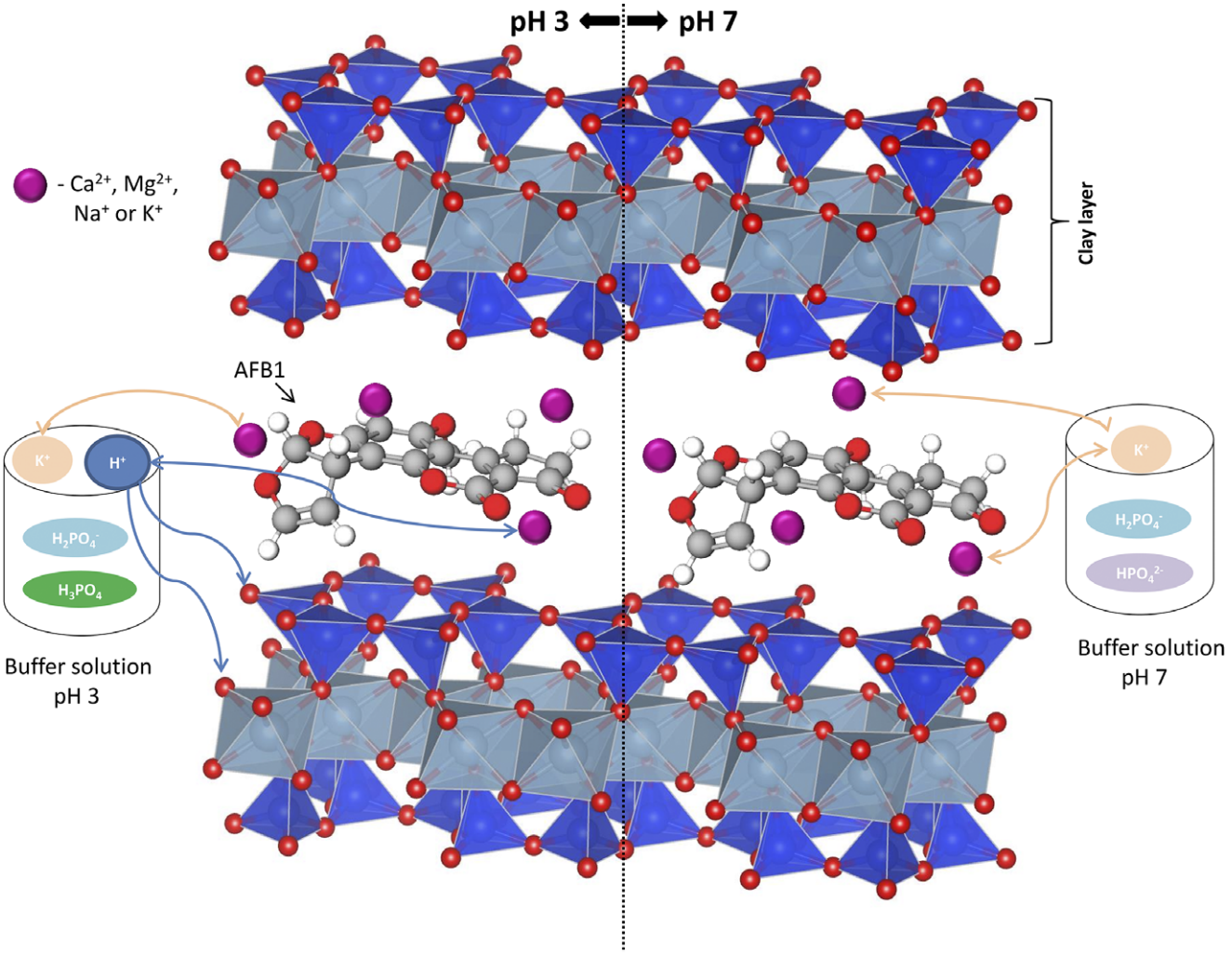



**Figure 6.** Schematic representation of AFB1 adsorption onto montmorillonite in buffers at pH 3 and 7. The structure of montmorillonite was generated in the *VESTA* program (Momma and Izumi, 2011) using parameters from Viani et al. (2002).

https://doi.org/10.1017/cmn.2026.10022 Published online by Cambridge University Press

montmorillonite content. In fact, the G-Clay possessed similar AFB1 adsorption capacities at both pH values. The other two Ca-bentonites (B-Clay and Y-Clay) showed much higher AFB1 capacities at pH 3 but similar capacities at pH 7 as the G-Clay. The Y-Clay had the largest montmorillonite content (98%), but this clay was of the *cis/trans* vacant type, which may cause slightly lower adsorption in comparison with the B-Clay, which was *cis*-vacant with a montmorillonite content of 83%. Enhanced AFB1 adsorption by *cis*-montmorillonites at pH 3 may be related to the position of octahedral OH groups that were on the same side of the octahedral site, meaning they were probably more available for interactions with protons from buffer solution, thereby creating protonated sites that can interact with AFB1. The opposing OH groups in *trans*-vacant montmorillonite (G-Clay) reduced the number and availability of sites for proton adsorption, thereby decreasing adsorption of AFB1 at pH 3. Thus, for the G-Clay at pH 3, only the exchangeable cations were available for AFB1 adsorption and its adsorption capacity was similar to that at pH 7. In addition, although it was expected that bentonites with a larger $SSA_{N2BET}$ value would exhibit greater AFB1 adsorption, comparison between the $SSA_{N2BET}$ values (Table 5) and AFB1 adsorption capacities (Table 6) at pH 3 and 7 showed that this was not the case. At pH 3, the AFB1 adsorption capacity of the Y-Clay (*cis/trans*-vacant, 98% of Ca-montmorillonite) was less than that of the B-Clay (*cis*-vacant, 83% Ca-montmorillonite), whereas its $SSA_{N2BET}$ was ~1.64 times greater than that of B-Clay. At pH 7, AFB1 adsorption capacities of these two bentonites were comparable but also did not correspond to the ratio of their specific surface areas. The lack of correlation between changes in AFB1 adsorption capacities and $SSA_{N2BET}$ was also evident for the G-Clay (*trans*-vacant, 88% Ca-montmorillonite) and P-Clay (*cis*-vacant, 63% Na/Ca montmorillonite). In summary, results confirmed that mineralogical, structural, chemical, and physico-chemical characteristics of smectite, all together, influenced AFB1 adsorption. In buffer solutions, ion exchange and AFB1 adsorption onto montmorillonites occurred simultaneously and exchangeable cations in the interlayer and at the surface, as well as protons adsorbed at the edges and in the interlayer under acidic conditions played an important role in AFB1 adsorption. In addition, the absence of plateaus in the measured AFB1 isotherms (Fig. 4) suggests that all exchangeable cations in montmorillonites were not fully saturated with AFB1 molecules. A summary of the adsorption of AFB1 onto bentonite(s) in buffer solutions is shown schematically in Fig. 6.

Finally, although all studied Ca-bentonites showed significant *in vitro* AFB1 adsorption in buffer solutions (Table 6) and fulfil the requirements of EU Regulation (in which an AFB1 binding capacity over 90% from a single *in vitro* AFB1 experiment is proposed for bentonite selection as an additive), an *in vivo* safety evaluation for application as AFB1 binding agents is also essential before inclusion in diets. So far, from the Ca-bentonites studied, only the G-Clay (raw and <5 μm fraction) was tested under *in vivo* conditions (Shannon et al., 2017). The addition of both adsorbents to the basal diet did not cause negative effects in any of the measured response variables, indicating that the G-Clay and concentrated G-Clay are safe to feed broiler chicks and will not negatively impact performance. Despite the fact that the <5 μm fraction of the G-Clay showed a greater AFB1 adsorption *in vitro* than the raw material (93.39 *vs* 79.30 mg $g^{-1}$), no large differences were observed between the two adsorbents with respect to reducing or preventing the toxic effects of AFB1, demonstrating that raw G-Clay was a very good AFB1 binding agent. In any case, although *in vitro* investigations are essential for understanding the mechanism of AFB1 adsorptions by bentonites, *in vivo* trials are necessary for their final selection as animal feed additives.

## Conclusions

Aflatoxin B1 (AFB1) adsorption onto three natural Ca-bentonites from the Balkan region (Beretnica, Serbia (B-Clay), Šipovo deposit, Bosnia (yellow clay: Y-Clay, and gray clay: G-Clay)) and one commercial pharmaceutical-grade Na/Ca bentonite (P-Clay) in phosphate buffer (pH 3 and 7) was correlated with mineralogical, structural, chemical, and physico-chemical properties of the bentonites as well as with their behavior in buffer solutions. All samples are composed dominantly of dioctahedral smectite (montmorillonite), although they differed in some mineralogical, structural, chemical, and physico-chemical properties. AFB1 adsorption by these bentonites increased with an increase in the initial toxin concentration, with greater adsorption observed at pH 3. The lowest adsorption of AFB1 occurred for the P-Clay at both pH values. The measured non-linear isotherms showed a slightly better fit with the Langmuir model.

The behavior of the bentonites in buffer solutions showed that a significant amount of native exchangeable cations was released from montmorillonite into solution within 30 min, being replaced with $K^+$ ions (at pH 3 and 7) and protons (pH 3) from buffers. In the presence of AFB1, ion exchange of native cations from the interlayer of montmorillonite and the surface with ions from buffers and AFB1 adsorption occurred simultaneously. Toxin adsorption capacities in buffers were related to the amounts of exchangeable cations in the montmorillonites during AFB1 adsorption in buffers. These results suggested that cations with the lowest ionic radius ($Mg^{2+}$ and $Ca^{2+}$) represented the primary active sites for AFB1 molecule adsorption, and when these sites were saturated with AFB1, adsorption continues by interaction with the hydration shells of monovalent cations. The affinity of cations toward AFB1 increased in the following order: $K^+ < Na^+ < Ca^{2+} < Mg^{2+}$. In addition, protons from the buffer solution at pH 3 caused protonation of edge groups in tetrahedral and octahedral sheets and they can also be adsorbed at the surfaces and in the interlayer, creating new sites that enhanced AFB1 adsorption. These mineralogical, structural, chemical, and physico-chemical characteristics of montmorillonites played important roles in AFB1 adsorption, but experimental conditions (e.g. composition of solution, initial AFB1 concentrations, contact time, etc.) also affect the overall adsorption process significantly.

**Supplementary material.** To view supplementary material for this article, please visit http://doi.org/10.1017/cmn.2026.10022.

**Author contribution.** Conceptualization, methodology, resources, writing original draft - review and Editing: A.D.; Investigation, writing - review and editing: M.M.; Investigation, formal analysis, visualization: M.Ož.; Writing - review and editing: G.E.R.; Investigation, formal analysis: M.Ob.; Investigation, writing - review and editing: D.K. and J.K.; Formal analysis, Investigation: D.S.; Investigation, visualization, writing - review and editing: D.L.B.

**Acknowledgements.** None.

**Financial support.** This research was supported by the Science Fund of the Republic of Serbia, grant no. 7748088, Project title: Composite clays as advanced materials in animal nutrition and biomedicine – AniNutBiomedCLAYs, and by the Ministry of Science, Technological Development and Innovation of the Republic of Serbia (contract number: 451-03-136/2025-03/200026). The companies Bentoproduct LLC from Šipovo, Bosnia, kindly provided bentonite

Y-Clay, and ZeoWorld LLC and Contractor LLC from Serbia kindly provided bentonite B-Clay.

**Competing interests.** The authors declare none.

**Data availability statement.** All data generated or analyzed during this study are included in this published article.

## References


Battilani, P., Toscano, P., Van Der Fels-Klerx, H. J., Moretti, A., Camardo Leggieri, M., Brera, C., Rortais, A., Goumperis, T., & Robinson, T. (2016). Aflatoxin $B_1$ contamination in maize in Europe increases due to climate change. *Scientific Reports*, *6*, 24328. https://doi.org/10.1038/srep24328

Bayram, H., Önal, M., Yılmaz, H., & Sarıkaya, Y. (2010). Thermal analysis of a white calcium bentonite. *Journal of Thermal Analysis and Calorimetry*, *101*, 873–879. https://doi.org/10.1007/s10973-009-0626-y

Belousov, P., Chupalenkov, N., Christidis, G. E., Zakusina, O., Zakusin, S., Morozov, I., Chernov, M., Zaitseva, T., Tyupina, E., & Krupskaya, V. (2021). Carboniferous bentonites from 10Th Khutor deposit (Russia): composition, properties and features of genesis. *Applied Clay Science*, *215*, 106308. https://doi.org/10.1016/j.clay.2021.106308

Bettiol, P. S., Cechinel, M. A. P., Oliveira, C. M., Goulart, K., Dol-Bó, A. G., Bernardin, A. M., & Peterson, M. (2022). Adsorption of aflatoxin $B_1$ mycotoxins by raw and lyophilized bentonitic clay. *Advanced Powder Technology*, *33*, 103682. https://doi.org/10.1016/j.apt.2022.103682

Chipera, S. J., Carey, J. W., & Bish, D. L. (1997). Controlled-humidity XRD analyses: application to the study of smectite expansion/contraction. In J. V. Gilfrich, J. C. Noyan, R. Jenkins, T. C. Huang, R. L. Snyder, D. K. Smith, M. A. Zaitz, & P. K. Predecki (eds), *Advances in X-Ray Analysis, vol. 39* (pp. 713–722). Plenum Press. https://doi.org/10.1154/S0376030800023168

D'Ascanio, V., Greco, D., Menicagli, E., Santovito, E., Catucci, L., Logrieco, A. F., & Avantaggiato, G. (2019). The role of geological origin of smectites and of their physico-chemical properties on aflatoxin adsorption. *Applied Clay Science*, *181*, 105209. https://doi.org/10.1016/j.clay.2019.105209

Daković, A., Matijašević, S., Rottinghaus, G. E., Ledoux, D. R., Butkeraitis, P., & Sekulić, Ž. (2008). Aflatoxin $B_1$ adsorption by natural and copper modified montmorillonite. *Colloids and Surfaces B: Biointerfaces*, *66*, 20–25. https://doi.org/10.1016/j.colsurfb.2008.05.008

Daković, A., Kragović, M., Rottinghaus, G. E., Ledoux, D. R., Butkeraitis, P., Vojislavljević, D. Z., Zarić, S. D., & Stamenić, L. (2012). Preparation and characterization of zinc-exchanged montmorillonite and its effectiveness as aflatoxin $B_1$ adsorbent. *Materials Chemistry and Physics*, *137*, 213–220. https://doi.org/10.1016/j.matchemphys.2012.09.010

Danková, Z., Mockovčiaková, A., & Dolinská, S. (2014). Influence of ultrasound irradiation on cadmium cations adsorption by montmorillonite. *Desalination and Water Treatment*, *52*, 5462–5469. https://doi.org/10.1080/19443994.2013.814006

Deng, Y., Velázquez, A. L. B., Billes, F., & Dixon, J. B. (2010). Bonding mechanisms between aflatoxin $B_1$ and smectite. *Applied Clay Science*, *50*, 92–98. https://doi.org/10.1016/j.clay.2010.07.008

Deng, Y., Liu, L., Velázquez, A. L. B., & Dixon, J. B. (2012). The determinative role of the exchange cation and layer-charge density of smectite on aflatoxin adsorption. *Clays and Clay Minerals*, *60*, 374–386. https://doi.org/10.1346/CCMN.2012.0600404

Desheng, Q., Fan, L., Yanhu, Y., & Niya, Z. (2005). Adsorption of aflatoxin $B_1$ on montmorillonite. *Poultry Science*, *84*, 959–961. https://doi.org/10.1093/ps/84.6.959

Dixon, J. B., Kannewischer, I., Tenorio Arvide, M. G., & Barrientos Velazquez, A. L. (2008). Aflatoxin sequestration in animal feeds by quality-labeled smectite clays: an introductory plan. *Applied Clay Science*, *40*, 201–208. https://doi.org/10.1016/j.clay.2007.10.010

Drits, V. A., & Zviagina, B. B. (2009). Trans-vacant and cis-vacant 2:1 layer silicates: structural features, identification, and occurrence. *Clays and Clay Minerals*, *57*, 405–415. https://doi.org/10.1346/CCMN.2009.0570401

Drits, V. A., Besson, G., & Muller, F. (1995). An improved model for structural transformations of heat-treated aluminous dioctahedral 2:1 layer silicates. *Clays and Clay Minerals*, *43*, 718–731. https://doi.org/10.1346/CCMN.1995.0430608

Dubinin, M. M. (1975). Physical adsorption of gases and vapors in micropores. In *Progress in Surface and Membrane Science* (vol. *9*). Academic Press Inc. https://doi.org/10.1016/b978-0-12-571809-7.50006-1

Emmerich, K., & Kahr, G. (2001). The cis- and trans-vacant variety of a montmorillonite: an attempt to create a model smectite. *Applied Clay Science*, *20*, 119–127. https://doi.org/10.1016/S0169-1317(01)00065-5

Escamilla-Roa, E., Hernández-Laguna, A., & Sainz-Díaz, C. I. (2014). Theoretical study of the hydrogen bonding and infrared spectroscopy in the cis-vacant polymorph of dioctahedral 2:1 phyllosilicates. *Journal of Molecular Modeling*, *20*, 1–15. https://doi.org/10.1007/s00894-014-2404-4

Et-Tayea, Y., Harrati, A., Rachid, A., Nasri, H., Attou, A., Arkame, Y., Manni, A., Mamouch, Y., El Bouari, A., El Khazanti, F., & Sadik, C. (2023). Mineralogical and physico-chemical characterization of bentonite materials from the Oued Zemmour area (Oriental Rif, Nador-Morocco): valorization in ceramic field. *Boletin de La Sociedad Espanola de Ceramica y Vidrio*, *62*, 268–283. https://doi.org/10.1016/j.bsecv.2022.03.001

**European Commission** (2013). Commission Implementing Regulation (EU) No. 1060/2013 of 29 October 2013 concerning the authorisation of bentonite as a feed additive for all animal species. *Official Journal of the European Union*, *L 289*, 33–37. http://irmm.jrc.ec.europa.eu/EURLs/EURL_feed_additives/Pages/index.aspx

Ferrage, E., Tournassat, C., Rinnert, E., & Lanson, B. (2005). Influence of pH on the interlayer cationic composition and hydration state of Ca-montmorillonite: analytical chemistry, chemical modelling and XRD profile modelling study. *Geochimica et Cosmochimica Acta*, *69*, 2797–2812. https://doi.org/10.1016/j.gca.2004.12.008

Gan, F., Hang, X., Huang, Q., & Deng, Y. (2019). Assessing and modifying China bentonites for aflatoxin adsorption. *Applied Clay Science*, *168*, 348–354. https://doi.org/10.1016/j.clay.2018.12.001

Goo, J. Y., Kim, B. J., Kwon, J. S., & Jo, H. Y. (2023). Bentonite alteration and retention of cesium and iodide ions by Ca-bentonite in alkaline and saline solutions. *Applied Clay Science*, *245*, 107141. https://doi.org/10.1016/j.clay.2023.107141

Grant, P. G., & Phillips, T. D. (1998). Isothermal adsorption of aflatoxin $B_1$ on HSCAS clay. *Journal of Agricultural and Food Chemistry*, *46*, 599–605. https://doi.org/10.1021/jf970604v

Grim, R. E., & Kulbicki, G. (1961). Montmorillonite: high temperature reactions and classification. *American Mineralogist*, *46*, 1329–1369.

Hofmann, H., Bauer, A., & Warr, L. N. (2004). Behavior of smectite in strong salt brines under conditions relevant to the disposal of low- to medium-grade nuclear waste. *Clays and Clay Minerals*, *52*, 14–24. https://doi.org/10.1346/CCMN.2004.0520102

**IARC Monographs on the Evaluation of Carcinogenic Risks to Humans** (1993). Vol. *56*, IARC, Lyon, France. https://doi.org/10.1136/jcp.48.7.691-a

Jabłońska, B., Busch, M., Kityk, A. V., & Huber, P. (2019). Clays – structural and surface properties and preliminary tests on copper sorption. *Minerals*, *9*, 704. https://doi.org/10.3390/min9110704

Kannewischer, I., Tenorio Arvide, M. G., Norman White, G., & Dixon, J. B. (2006). Smectite clays as adsorbents of aflatoxin $B_1$: initial steps. *Clay Science*, *12* (suppl2), 199–204. https://doi.org/10.11362/jcssjclayscience1960.12.Supplement2_199

Kaufhold, S., Dohrmann, R., Klinkenberg, M., Siegesmund, S., & Ufer, K. (2010). $N_2$-BET specific surface area of bentonites. *Journal of Colloid and Interface Science*, *349*, 275–282. https://doi.org/10.1016/j.jcis.2010.05.018

Kaufhold, S., Plötze, M., Klinkenberg, M., & Dohrmann, R. (2013). Density and porosity of bentonites. *Journal of Porous Materials*, *20*, 191–208. https://doi.org/10.1007/s10934-012-9589-7

Kirschenbaum, H. (1983). The classical chemical analysis of silicate rocks – the old and the new. In *US Geological Survey Bulletin*. Geological Survey Bulletin 1547, United States Government Printing Office, Washington.

Lacerda, E. H. C., Lacerda, L. H. da S., Andrade, A. V. C. de, Fujiwara, S. T., & Kloss, J. R. (2023). Spectroscopic, mineralogical and photocatalytic characterization of bentonite clay: a jointed DFT and experimental approach. *Journal of Photochemistry and Photobiology A: Chemistry*, *445*, 115077. https://doi.org/10.1016/j.jphotochem.2023.115077

Li, Y., Tian, G., Gong, L., Chen, B., Kong, L., & Liang, J. (2020). Evaluation of natural sepiolite clay as adsorbents for aflatoxin $B_1$: a comparative study. *Journal of Environmental Chemical Engineering*, *8*, 104052. https://doi.org/10.1016/j.jece.2020.104052

Lian, C., Wang, G., Lv, W. Q., Sun, Z., & Zheng, S. (2019). Effect of calcination temperature on the structure of chitosan-modified montmorillonites and their adsorption of aflatoxin $B_1$. *Clays and Clay Minerals*, *67*, 357–366. https://doi.org/10.1007/s42860-019-00042-z

Liu, J. H., Cai, W. K., Khatoon, N., Yu, W. H., & Zhou, C. H. (2021). On how montmorillonite as an ingredient in animal feed functions. *Applied Clay Science*, *202*, 105963. https://doi.org/10.1016/j.clay.2020.105963

Mannu, A., Vlachopoulou, G., Sireus, V., Mulas, G., & Petretto, G. L. (2019). Characterization of Sardinian Bentonite. *Journal of Scientific Research*, *11*, 145–150. https://doi.org/10.3329/jsr.v11i1.36900

Marcus, Y. (1991). Thermodynamics of solvation of ions. *Journal of the Chemical Society, Faraday Transactions*, *87*, 2995–2999. https://doi.org/10.1039/FT9918702995

Marroquín-Cardona, A., Deng, Y., Taylor, J. F., Hallmark, C. T., Johnson, N. M., & Phillips, T. D. (2009). *In vitro* and *in vivo* characterization of mycotoxin-binding additives used for animal feeds in Mexico. *Food Additives and Contaminants - Part A Chemistry, Analysis, Control, Exposure and Risk Assessment*, *26*, 733–743. https://doi.org/10.1080/02652030802641872

Marroquín-Cardona, A. G., Deng, Y., Garcia-Mazcorro, J. F., Johnson, N. M., Mitchell, N. J., Tang, L., Wang, J. S., Harvey, R. B., & Phillips, T. D. (2022). Aflatoxin $B_1$ sorption and safety of dietary sodium bentonite in Sprague-Dawley rats. *Clays and Clay Minerals*, *70*, 165–181. https://doi.org/10.1007/s42860-022-00173-w

Merchant, H. A., McConnell, E. L., Liu, F., Ramaswamy, C., Kulkarni, R. P., Basit, A. W., & Murdan, S. (2011). Assessment of gastrointestinal pH, fluid and lymphoid tissue in the guinea pig, rabbit and pig, and implications for their use in drug development. *European Journal of Pharmaceutical Sciences*, *42*, 3–10. https://doi.org/10.1016/j.ejps.2010.09.019

Metz, V., Amram, K., & Ganor, J. (2005). Stoichiometry of smectite dissolution reaction. *Geochimica et Cosmochimica Acta*, *69*, 1755–1772. https://doi.org/10.1016/j.gca.2004.09.027

Milonjić, S. K. (2007). A consideration of the correct calculation of thermodynamic parameters of adsorption. *Journal of the Serbian Chemical Society*, *72*, 1363–1367. https://doi.org/10.2298/JSC0712363M

Missana, T., Alonso, U., Fernández, A. M., & García-Gutiérrez, M. (2018). Analysis of the stability behaviour of colloids obtained from different smectite clays. *Applied Geochemistry*, *92*, 180–187. https://doi.org/10.1016/j.apgeochem.2018.03.010

Momma, K., & Izumi, F. (2011). *VESTA 3* for three-dimensional visualization of crystal, volumetric and morphology data. *Journal of Applied Crystallography*, *44*, 1272–1276. https://doi.org/10.1107/S0021889811038970

Musso, T. B., Pettinari, G., Pozo, M., Roca Jalil, M. E., & González Gil-García, R. (2022). A new deposit of Na-bentonite from the Upper Cretaceous Anacleto Formation (Neuquén Basin, Argentina): characterization and properties. *Applied Clay Science*, *220*, 106461. https://doi.org/10.1016/j.clay.2022.106461

Nagy, N. M., Kónya, J., & Urbin, Z. (1997). The competitive exchange of hydrogen and cobalt ions on calcium-montmorillonite. *Colloids and Surfaces A: Physicochemical and Engineering Aspects*, *121*, 117–124. https://doi.org/10.1016/S0927-7757(96)03844-7

Noyan, H., Önal, M., & Sarikaya, Y. (2006). The effect of heating on the surface area, porosity and surface acidity of a bentonite. *Clays and Clay Minerals*, *54*, 375–381. https://doi.org/10.1346/CCMN.2006.0540308

Oguz, H., Bahcivan, E., Erdogan, T., Yalcin, N. F., Ozdas, A., Isık, M. K., & Altunbas, O. (2022). *In vitro* mycotoxin binding capacities of clays, glucomannan and their combinations. *Toxicon*, *214*, 93–103. https://doi.org/10.1016/j.toxicon.2022.05.006

Ožegović, M., Marković, M., Daković, A., Obradović, M., Smiljanić, D., Rottinghaus, G. E., Jaćević, V., Ignjatović, L., & Sredović Ignjatović, I. (2025). Assessment of nontoxic surfactant-modified kaolinite for potential application as an adsorbent for mycotoxins. *Minerals*, *15*, 731.

Phillips, T. D., Afriyie-Gyawu, E., Williams, J., Huebner, H., Ankrah, N. A., Ofori-Adjei, D., Jolly, P., Johnson, N., Taylor, J., Marroquin-Cardona, A., Xu, L., Tang, L., & Wang, J. S. (2008). Reducing human exposure to aflatoxin through the use of clay: a review. *Food Additives and Contaminants - Part A Chemistry, Analysis, Control, Exposure and Risk Assessment*, *25*, 134–145. https://doi.org/10.1080/02652030701567467

Phillips, T. D., Kubena, L. F., Harvey, R. B., Taylor, D. R., & Heidelbaugh, N. D. (1988). Hydrated sodium calcium aluminosilicate : a high affinity sorbent for aflatoxin. *Poultry Science*, *67*, 243–247. https://doi.org/10.3382/ps.0670243

Phillips, T. D., Bashir Sarr, A., & Grant, P. G. (1995). Selective chemisorption and detoxification of aflatoxins by phyllosilicate clay. *Natural Toxins*, *3*, 204–213. https://doi.org/10.1002/nt.2620030407

Qiao, Z., Liu, Q., Zhang, S., & Wu, Y. (2019). The mineralogical characteristics between opaline silica in bentonite and α-cristobalite. *Solid State Sciences*, *96*, 105948. https://doi.org/10.1016/j.solidstatesciences.2019.105948

Rehman, M. U., Manan, A., Uzair, M., Khan, A. S., Ullah, A., Ahmad, A. S., Wazir, A. H., Qazi, I., & Khan, M. A. (2021). Physicochemical characterization of Pakistani clay for adsorption of methylene blue: kinetic, isotherm and thermodynamic study. *Materials Chemistry and Physics*, *269*, 124722. https://doi.org/10.1016/j.matchemphys.2021.124722

Rouquerol, F., Rouquerol, J., & Sing, K. (1999). *Adsorption by Powders and Porous Solids: Principles, Methodology and Applications*. Academic Press, New York.

Rouquerol, J., Llewellyn, P., & Rouquerol, F. (2007). Is the BET equation applicable to microporous adsorbents? In *Studies in Surface Science and Catalysis* (vol. *160*). Elsevier B.V. https://doi.org/10.1016/s0167-2991(07)80008-5

Şans, B. E., Güven, O., Esenli, F., & Çelik, M. S. (2017). Contribution of cations and layer charges in the smectite structure on zeta potential of Ca-bentonites. *Applied Clay Science*, *143*, 415–421. https://doi.org/10.1016/j.clay.2017.04.016

Schultz, L. G. (1969). Lithium and potassium absorption, dehydroxylation temperature, and structural water content of aluminous smectites. *Clays and Clay Minerals*, *17*, 115–149. https://doi.org/10.1346/CCMN.1969.0170302

Shannon, T. A., Ledoux, D. R., Rottinghaus, G. E., Shaw, D. P., Daković, A., & Marković, M. (2017). The efficacy of raw and concentrated bentonite clay in reducing the toxic effects of aflatoxin in broiler chicks. *Poultry Science*, *96*, 1651–1658. https://doi.org/10.3382/ps/pew408

Shwan, D. M. S., Qadr, F. M., Kaufhold, S., & Ufer, K. (2023). Exploration and characterization of local raw bentonite of a part of Garmiyan-Kurdistan/Iraq. *Kuwait Journal of Science*, *50*, 731–738. https://doi.org/10.1016/j.kjs.2023.07.006

Sing, K. S. W., & Williams, R. T. (2004). Physisorption hysteresis loops and the characterization of nanoporous materials. *Adsorption Science and Technology*, *22*, 773–782. https://doi.org/10.1260/0263617053499032

Siri-anusornsak, W., Meneely, J., Greer, B., Vangnai, K., Mahakarnchanakul, W., Elliott, C., Petchkongkaew, A., & Kolawole, O. (2023). *In vitro* assessment of commercial multi-mycotoxin binders to reduce the bioavailability of emerging mycotoxins in livestock. *Emerging Contaminants*, *9*, 100256. https://doi.org/10.1016/j.emcon.2023.100256

Sun, Z., Lian, C., Li, C., & Zheng, S. (2020). Investigations on organo-montmorillonites modified by binary nonionic/zwitterionic surfactant mixtures for simultaneous adsorption of aflatoxin $B_1$ and zearalenone. *Journal of Colloid and Interface Science*, *565*, 11–22. https://doi.org/10.1016/j.jcis.2020.01.013

Tanyol, M., Yonten, V., & Demir, V. (2015). Removal of phosphate from aqueous solutions by chemical- and thermal-modified bentonite clay. *Water, Air, and Soil Pollution*, *226*. https://doi.org/10.1007/s11270-015-2538-8

Tenorio Arvide, M. G., Mulder, I., Barrientos Velazquez, A. L., & Dixon, J. B. (2008). Smectite clay adsorption of aflatoxin vs. octahedral composition as indicated by FTIR. *Clays and Clay Minerals*, *56*, 571–578. https://doi.org/10.1346/CCMN.2008.0560510

Thommes, M., Kaneko, K., Neimark, A. V., Olivier, J. P., Rodriguez-Reinoso, F., Rouquerol, J., & Sing, K. S. W. (2015). Physisorption of gases, with special reference to the evaluation of surface area and pore size distribution (IUPAC Technical Report). *Pure and Applied Chemistry*, *87*, 1051–1069. https://doi.org/10.1515/pac-2014-1117

Vekiru, E., Fruhauf, S., Sahin, M., Ottner, F., Schatzmayr, G., & Krska, R. (2007). Investigation of various adsorbents for their ability to bind Aflatoxin $B_1$. *Mycotoxin Research*, *23*, 27–33. https://doi.org/10.1007/BF02946021

https://doi.org/10.1017/cmn.2026.10022 Published online by Cambridge University Press

Vekiru, E., Fruhauf, S., Rodrigues, I., Ottner, F., Krska, R., Schatzmayr, G., Ledoux, D. R., Rottinghaus, G. E., & Bermudez, A. J. (2015). *In vitro* binding assessment and *in vivo* efficacy of several adsorbents against aflatoxin $B_1$. *World Mycotoxin Journal*, *8*, 477–488. https://doi.org/10.3920/WMJ2014.1800

Viani, A., Gualtieri, A. F., & Artioli, G. (2002). The nature of disorder in montmorillonite by simulation of X-ray powder patterns. *American Mineralogist*, *87*, 966–975. https://doi.org/10.2138/am-2002-0720

Wang, G., Miao, Y., Sun, Z., & Zheng, S. (2018). Simultaneous adsorption of aflatoxin $B_1$ and zearalenone by mono- and di-alkyl cationic surfactants modified montmorillonites. *Journal of Colloid and Interface Science*, *511*, 67–76. https://doi.org/10.1016/j.jcis.2017.09.074

Wang, T. H., Liu, T. Y., Wu, D. C., Li, M. H., Chen, J. R., & Teng, S. P. (2010). Performance of phosphoric acid activated montmorillonite as buffer materials for radioactive waste repository. *Journal of Hazardous Materials*, *173*, 335–342. https://doi.org/10.1016/j.jhazmat.2009.08.091

Wolters, F., & Emmerich, K. (2007). Thermal reactions of smectites-relation of dehydroxylation temperature to octahedral structure. *Thermochimica Acta*, *462*, 80–88. https://doi.org/10.1016/j.tca.2007.06.002

Zhao, C., Wang, C., Hong, H., Algeo, T. J., Yin, K., Ji, K., Song, B., Abels, H. A., & Christidis, G. E. (2021). Origin of dioctahedral smectites in Lower Eocene Lulehe Formation paleosols (Qaidam Basin, China). *Applied Clay Science*, *203*, 106026. https://doi.org/10.1016/j.clay.2021.106026

https://doi.org/10.1017/cmn.2026.10022 Published online by Cambridge University Press